VERTICAL AXIS WIND TURBINE
USING SAILS

by

T.M. NGABO

A Thesis submitted to the Faculty of Graduate Studies and Research in partial fulfillment of the requirements for the degree of Master of Engineering.

Department of Mechanical Engineering
McGill University
Montreal, Quebec, Canada

April, 1978

SUMMARY

This study is an extension of an earlier one by J. Robert on the feasibility of using sail blades on vertical axis wind turbines. A three bladed wind turbine 9 ft. high by 6 ft. diameter was tested in a 15 ft. diameter open jet vertical wind tunnel for Reynolds numbers based on diameter ranging from 5.6×10^5 to 7.9×10^5. The turbine had a high solidity of 1.4 and as a result the operating range of tip speed ratios was from 0 to about 2.5.

Two types of sail blades were tested. One consisted of two layers of Dacron sail cloth wrapped around a circular leading edge dowel while the other was a single Dacron sheet or jib with the leading edge held by a taut braided wire. The turbine when fitted with double sail blades was found to be self-starting at low trailing edge pre-tensions. In both cases the maximum power output was about half of that normally obtained with vertical axis wind turbines fitted with solid aerofoil blades operating at tip speed ratios ranging from 0 to 6.

Due to the simplicity of the design, it is anticipated that the cost and know-how required to manufacture the turbine would be low. As a result, the turbine would be ideal for use in developing nations, where it could have wide applications for small jobs requiring a power of 1 kW.

RESUME

Cette étude est un développement d'une investigation antérieure de J. Robert portant sur la possibilité d'employer des voiles comme pales dans les turbines à air. Une turbine a trois pales mesurant 9 p. de longue et 6 p. de diamètre a été testée dans une soufflerie ouverte de 15 p. de diamètre pour des nombres de Reynolds basés sur la diamètre allant de 5.6×10^5 à 7.9×10^5. La turbine avait une grande surface de pale par rapport à la surface balayée (rapport: 1.4) et, par conséquent, l'étendue des rapports de vitesse aux extrémités variait de 0 à environ 2.5.

Deux types de voiles ont été essayés. La première était faite de deux couches de Dacron entourant un goujon circulaire périphérique alors que la seconde était constituée d'une seule couche de Dacron (foc) dont un des bords était tendu par un fil métallique tressé. Quand la turbine avait pales doubles elle était autodébutante à des pré-tensions de traîne périphérique peu élevées. Dans les deux cas, le rendement maximum était environ la moitié de celui normalement obtenu avec des turbines à axe vertical, équippées de pales à voilure solide dont les rapports de vitesse aux extrémités variaient entre 0 et 6.

Dû à la simplicité de la conception, on anticipe que le coût et les connaissances requises pour manufacturer la turbine seraient bas. Par conséquent, la turbine serait idéale pour les pays en voie de développement où elle pourrait connaître des applications multiples pour de petits travaux nécessitant une énergie de 1 kW.

ACKNOWLEDGEMENTS

The author wishes to particularly thank his research director Professor B.G. Newman for his great help, interest and guidance throughout the author's stay at McGill. Professor Newman also designed the wind turbine which was tested. The author thanks Mr. Joe Dubik who built the turbine and ancillary apparatus, Mr. Jack Templin of the National Aeronautical Establishment who arranged for the use of the 15 ft. diameter vertical tunnel and Mr. Peter South who provided helpful advice and his dynamometer for measuring the turbine torque. Thanks are also due to Mr. Harvey Reimer who helped run the experiment at the National Research Council and Mr. Jean Robert, whose computer program was used in the simulation of the turbine performance.

The author offers special thanks to the Canadian Commonwealth Scholarship and Fellowship Committee. Above all, the author thanks his wife for having given him encouragement and strength through her constant letters, and Mrs. Maxine Kazakoff who did the typing of this report.

The work was supported by the National Research Council on Grant No. A7096 (Grantee: Prof. B.G. Newman) and Quebec DGES under FCAC Grant entitled "L'Energie Eolienne: Source d'Energie Renouvelable" (Grantee: Prof. M.P. Paidoussis).

TABLE OF CONTENTS

NOTATION

(Symbols not included in the Notation list are defined in the text.)

A	Frontal swept area of the wind turbine
A_s	Area of one sail blade
b	Length of leading edge dowel
c	Chord of a blade or strut
$\bar{c} = \frac{A_s}{2b}$	Mean chord
c_R	Chord of blade at maximum radius R
$C_D = \frac{D}{\frac{1}{2}\rho c V^2}$	Drag coefficient of strut section
$C_D = \frac{D}{\frac{1}{2}\rho A V^2}$	Disc drag coefficient based on ambient wind speed
$C_{D_{PL}}$	Drag coefficient of a fully solid turbine
$C_M = \frac{2M}{\frac{1}{2}\rho \Omega^2 R^5}$	Moment coefficient of a rotating disc
$C_P = \frac{P}{\frac{1}{2}\rho A V^3}$	Wind turbine power coefficient
Cp_{max}	Maximum power coefficient
$C_Q = \frac{Q}{\frac{1}{2}\rho A R V^2}$	Wind turbine starting torque coefficient
$C_T = \frac{T}{\frac{1}{2}\rho A_s V^2}$	Pre-tension coefficient
$C_X = \frac{X}{\frac{1}{2}\rho c U^2}$	Coefficient of the aerodynamic force on the blade in the direction of the chord

$C_Y = \frac{Y}{\frac{1}{2}\rho c U^2}$	Coefficient of the aerodynamic force on the blade in the direction perpendicular to the chord
d	Diameter of leading edge dowel
D	Drag of wind turbine or strut
e	Force per unit width of the sail for each piece of cloth required to produce unit strain in the sail in the direction of the chord
E	Force required to produce unit strain
E_L	Force required to produce unit strain in the luff
E_T	Force required to produce unit strain in the leech
E_Y	Young's Modulus of the shaft
I	Moment of inertia of shaft about a diameter
ℓ	Length of the trailing edge of the blade when wind loaded
ℓ_0	Unstretched length of the trailing edge of the blade
ℓ_T	Length of the trailing edge after pre-tension with wind off
L	Length of the turbine shaft
m	Mass of the shaft per unit length
M	Moment of one side for a rotating disc
M_c	Concentrated mass at the centre of the shaft

N	Number of blades or struts
$\frac{Nc_R}{R}$	Wind turbine solidity
P	Wind turbine power output
Q	Wind turbine starting torque
r	Local radius of a strut for any azimuthal position
R	Maximum radius of the wind turbine
$Re = \frac{\rho V(2R)}{\mu}$	Wind turbine Reynolds number based on maximum diameter
s	Radius of curvature of trailing edge when wind loaded
T	Tension force with wind load
T_L	Pre-tension force in the luff wire for single sail blades
T_T	Pre-tension force in the leech line
U	Net air velocity relative to the blade section
v	Normal velocity through sail blade material associated with a pressure difference Δp
V	Ambient wind speed with solid blockage correction
V_D	Actuator disc velocity
V_t	Tunnel speed without solid blockage correction

W	Work done against drag of one strut in one revolution
x	Trailing edge leech hollow with wind load
x_T	Original leech hollow after pre-tensioning without wind load
X	Chordwise aerodynamic force on the trailing edge per unit span of sail
Y	Aerodynamic force on the trailing edge normal to the blade chord per unit span of sail
$z = \frac{r}{R}$	Ratio of local radius of strut to maximum radius
δ	Extension of the sail chordwise after pre-tension with wind off
ΔCp	Loss of power coefficient associated with the central disc
Δp	Pressure difference across a sail blade
ε	Change in angle of attack when sail blade is wind loaded
ε_s	Solid blockage correction factor for wind tunnel measurements
η	Angle as defined in Fig. A-2
θ	Azimuthal angle of strut
$\lambda = \frac{\Omega R}{V}$	Tip speed ratio of wind turbine
μ	Air viscosity

ν	Shape factor in the expression for solid blockage correction
ρ	Air density
ρ_d	Density of leading edge dowel
σ	Mass of the sail cloth per unit area
σ_y	Ultimate stress of leading edge dowel
τ	A factor in solid blockage correction depending on the shape of the cross-sectional area of the tunnel and the nature of its boundary
ϕ	An angle as defined in Fig. A-1
Ω	Angular velocity of the wind turbine
Ω_1	First critical speed of shaft
Ω_2	First critical speed due to a central concentrated mass on the shaft
Ω_c	Resultant first critical speed of the turbine

Subscripts

L	Applies to pre-tension in the luff wire
T	Applies to pre-tension in the leech

1. INTRODUCTION

The extravagant use of fossil fuels will eventually lead to a shortage of energy and therefore renewable sources are of increasing importance. Research has thus been undertaken to find alternative sources of energy. Windmills or wind turbines have been used in most parts of the world. The earliest of these machines were of the horizontal axis type and some of them like the ancient Greek and Portuguese wind turbines used sails [1]. Although they are simple to construct and can be furled in high winds their efficiencies are low and if the wind changes direction they have to be realigned with the new wind direction. The later Dutch and English wind turbines also used sail cloth on a wooden lattice to form more sophisticated furlable blades.

The vertical axis machines of the Savonius and Darrieus types have the advantage over the horizontal machines in that they are insensitive to the wind direction. The Savonius type is usually impractical in sizes that produce power of about 1 kW, due to their excessive use of material and high weight. They typically give about 0.1 kW [2]. The Darrieus wind turbine, as re-invented by Rangi and South at the National Aeronautical Establishment in Canada, was originally patented by J.M. Darrieus in France in the 1920's. This type of wind turbine has been built in large sizes to give power outputs of up to 200 kW but this is probably not the limiting power this type of wind turbine can produce. The 200 kW Darrieus wind turbine has been built in Canada on the Magdalene Islands in the St. Lawrence Gulf [3, 4, 5].

Nevertheless in some of the developing countries due to the level of prevailing technology even wind turbines have not been used extensively. Parkes and van de Laak [6] note for instance that in Tanzania, only thirty wind turbines have been found and most of them are no longer in use notwithstanding the fact that wind speeds average up to 16 mph in most parts of the country. Possibly what is needed is a cheap machine which can be built and repaired at the local village level.

There are two distinct advantages of the vertical axis wind turbines over the horizontal axis ones, namely:

1) The vertical axis wind turbine is insensitive to the wind direction. The horizontal axis machine requires re-alignment if the wind changes direction.
2) The vertical axis machine requires a smaller tower size to support it because the top bearing may be supported by guy wires.

Efforts have been made at McGill University to develop the Darrieus type wind turbine to suit technologies of the developing nations of the world. Instead of solid metal blades, sail cloth material was used. A model version of this wind turbine with sail blades was tested by Robert [7]. In his tests, Robert used a 9 in. high "two-dimensional" model with parallel blades supported between two thin aluminum discs, 11.5 in. diameter. The blades were of constant chord. Using computer simulation, Robert showed that the following specifications would give a design which could be close to the optimum:

1) Impervious sail cloth such as Dacron should be used.
2) The solidity of the wind turbine should be close to one. With a high solidity the turbine runs at low tip speed ratios and high bending moment stresses in the leading edge dowels due to centrifugal loads are hence reduced.
3) Three sail blades to obtain self-starting for any wind direction.

The present study involved testing two wind turbine models which were designed to meet the specifications for optimum output established by Robert. One was a smaller model 16 in. high and 11.5 in. maximum diameter while the other was a much bigger model 9 ft. high and 6 ft. in diameter. The smaller model consisted of 3 blades inclined at 30° to the vertical axis of rotation and was tested in the McGill 3' x 2' wind tunnel with a closed working section. The tests on the smaller model were performed at a Reynolds number of 2.2×10^5 based on the turbine maximum diameter and for constant trailing edge tensions. Due to structural limitations, this model could only be run at the low Reynolds number quoted above. The wind turbine was however self-starting.

The bigger wind turbine model was tested in Ottawa in a 15 ft. open jet vertical tunnel. It had three blades inclined at an angle of 30° to the axis of rotation. Two types of sail blade were tested with this model. One was a double sail formed by wrapping the sail around a circular wooden leading edge dowel; while the second type of sail was a single flat sheet of sail cloth or simple jib. The leading edge of the single sail was kept very taut by a braided steel wire under high tension which kept the leading edge nearly straight under load. The single sail had the same overall dimensions as the double sail.

Tests on both the double sail and single sail turbines were preformed at wind turbine Reynolds numbers based on the turbine maximum diameter ranging from 5.6×10^5 to 7.9×10^5. For the double sail blades the trailing edge tension was varied and the trailing edge elasticity altered in some tests. For the single sail both the leading edge and trailing edge tensions were varied during the tests.

2. DESCRIPTION OF THE TEST TURBINE

The wind turbine design was based on the recommendations of Robert [7]. Its size was designed to be as large as possible for a 15 ft. diameter open jet wind tunnel consistent with keeping the wind tunnel interference corrections on the speed to about 1%. The turbine was 9 ft. high and about 6 ft. central diameter. The central shaft was an aluminum pipe 1.36 in. internal diameter and 1.66 in. outside diameter. Aluminum was chosen to keep down the weight. The central disc was made from plywood 0.7 in. thick and mounted on the axis shaft by means of two small aluminum flanges (Fig. 1). The disc was lightened by cut-outs in the lightly stressed sections to reduce its weight and the possibility of whirling at operating speeds. The cut-outs were covered by doped cotton fabric. The end discs were made of plywood 0.7 in. thick and about 1 ft. diameter, mounted on small threaded aluminum flanges. Pins were used to locate all the flanges relative to the shaft at the appropriate azimuthal positions.

The double sail blades were made of Dacron fabric of density 3 oz. per square yard wrapped round a wooden leading edge dowel of diameter 1 3/8 in. The blades had symmetrical aerofoil cross-sections. The dowels were inclined at an angle of 30° to the axis of rotation. This angle would be suitable for supporting the top bearing by guy wires in the case of a field application. The sails tapered from 16.5 in. at the equatorial diameter to 8.5 in. at each end, giving a taper ratio of about 2 to 1 and an average thickness to chord ratio of 11%. The chord line of the blades was in the direction of the cloth warp. The trailing edge of the sail blades was hollowed in order to facilitate tensioning the sail. The average maximum leech line hollow of the blades was 1.95 in., which was 3% of the sail length, and is a ratio conventionally used on yacht sails (Fig. 2). The leech was a 3/32 in. diameter Dacron line running through a seam in the sail at the trailing edge. For one set of tests, the leech line was sewn to the sail in the seam thereby effectively decreasing the trailing edge elasticity. The application of the trailing edge tension was by means of a torque wrench which wound each leech line on a small ratchet mounted drum. Each drum assembly was made from a ratchet socket wrench: an aluminum pulley of diameter 1.5 in. tight fitted to the outside of the socket and a bolt glued to the inside was mounted on a supporting bracket. The bracket was fixed on the outside of one end disc of the turbine (Fig. 3b). The cloth on the double sail blades was cut in such a way that the blades were continuous on the outside while the inside was separated into two parts at the largest radius of the turbine. Each sail blade was reinforced at its edges and ends. The outside part of the sail rested tangentially on the central disc at the centre, and the inner, separated, parts of the sail were laced together by a Dacron line which passed through eyelets (grommets) in the sail and holes drilled in the central disc. The lacing was tight enough to eliminate creases on the inside part of the sail.

The single sail was a flat sheet of Dacron cloth. The leading edge or luff was tensioned through a 3/32 in. diameter braided wire, the tensioning being done by a screw mechanism similar to that used on cable brakes of bicycles (Fig. 4b). The single sail had almost the same overall dimensions of chord length, taper ratio and trailing edge geometry as the double sail blade (Fig. 2). The tensioning of the trailing edges was done in the same was as for the double sail (Fig. 4c). The single sail was made in two parts with the braided wire running through a seam in the leading edge of both parts and the Dacron line running through another seam in the trailing edge. The two parts were laced through eyelets to holes in the central disc. Both the trailing edge and the leading edge of the single sail were reinforced.

The whole turbine structure was mounted on two self-aligning ball bearings. The bearings were fitted into rectangular metal blocks which were in turn attached to the tunnel mounting arms, so that it was possible to swing the turbine out of the tunnel stream to make adjustments (Figs. 3a, 4a).

3. DESCRIPTION OF THE ANCILLARY APPARATUS

The experiment was performed at the National Aeronautical Establishment, Ottawa in the 15 ft. diameter open jet 'spinning' tunnel. The tunnel has an upward flowing airstream and the turbine was therefore mounted horizontally in it. The tunnel is run by a 250 hp motor and the speed ranges from 0 to 80 ft/sec. The tunnel speed was determined by measuring the reference pressure in the settling chamber relative to the pressure in the working section, which was taken as atmospheric.

The wind turbine angular velocity was determined by the use of an electronic counter and an instrument composed of a photocell and a light bulb. Cutting off the illumination from reaching the photocell activated a pulse which could be picked up by the electronic counter. A thin disc with 18 equally spaced holes was mounted on the wind turbine shaft between one end disc and the bearing block (Figs. 3b, 4c). The complete instrument was mounted on the bearing block. When the wind turbine rotated, the thin disc interrupted the light beam and the pulses activated by the photocell were recorded by the electronic counter.

A pulley on the wind turbine shaft connected it to a 1 hp 220 volts 1800 rpm 3 phase synchronous motor through a vee-belt system giving a speed increase of 6 to 1. The motor acted as a load on the turbine, and was run as a generator through a variable frequency supply of a Ward Leonard system, driving a rotary transformer with the secondary windings connected to the 60 Hz mains supply. It was a power absorbing system which could operate at nearly fixed frequency for each setting even at relatively low tip speed ratios. The driven motor was fixed below the bearing block and can be seen in Figs. 3b and 4c.

To measure the output torque, the turbine shaft was connected to a 1/4 in. diameter 5 ft. long steel rod placed inside an equally long outer tube about 2 in. outside diameter and was firmly attached to it at the far end. The outer tube was bolted to the pulley (Figs. 3b, 4c). The torque output from the turbine was therefore measured as the relative rotation between the shaft and the pulley during the rotation of the wind turbine. A pointer indicated this relative rotation on a scale mounted on top of the pulley and was viewed using a synchronized stroboscopic light. The output torque was calculated from earlier static torque calibrations of the assembly using dead weights. Both the speed counter and the dynamometer were mounted on the same end of the shaft (Figs. 3b, and 4c).

A tension meter for measuring tension in aircraft wires and cables was used to measure the tension in the luff wire. The instrument applied a cross-load to the wire and the accompanying deflection was measured.

4. EXPERIMENTAL PROCEDURE

With the turbine swung out of the tunnel, the required tension in the leech line was applied before each test using the torque wrench. When tensioning the leech line it was necessary to make sure that the applied tension was uniform throughout its length. To facilitate this, the slot in the central disc through which the leech line passed had to be waxed occasionally to reduce friction. The central disc was also oscillated back and forth manually to equalize the tension on both sides. For the single sail the luff wire was also tensioned before each test.

A zero reading of the dynamometer was taken before each test. After setting the required tensions in the leech line (and the luff wire in the case of the single sail), the wind turbine was swung into the tunnel. The tunnel was run at a specified dynamic pressure for each frequency setting of the motor which ran as a generator for most of the readings, and was adjusted to vary over the working range. The wind turbine torque and angular velocity were measured for a variety of loads obtained by changing the frequency settings of the motor generator 'supply'. The tunnel reference pressure and ambient air pressure were also noted for each test. The tests were repeated for other tunnel speeds and leading and trailing edge tensions and elasticities. The free-wheeling tests were performed at zero load with the vee-belt removed from the dynamometer, and were made for a wider range of tunnel speeds.

5. EXPERIMENTAL RESULTS

5.1 Identification of the Relevant Non-dimensional Coefficients

For a specific turbine geometry the following coefficients were identified as being sufficient to define the operating conditions of the wind turbine:

1. The Reynolds number based on the maximum diameter of the wind turbine.

$$Re = \frac{\rho V(2R)}{\mu}$$

where

ρ is the density of air

V is the tunnel speed corrected for solid blockage

R is the central radius of the turbine

μ is the dynamic viscosity of air.

2. The wind turbine tip-speed ratio

$$\lambda = \frac{\Omega R}{V}$$

where

Ω is the angular velocity of the wind turbine.

3. A non-dimensional leech-line pre-tension coefficient,

$$C_{TT} = \frac{T_T}{\frac{1}{2}\rho V^2 A_S}$$

where

T_T is the pre-tension force in the leech-line

A_S is the area of one complete sail blade.

4. A non-dimensional luff-wire pre-tension coefficient,

$$C_{TL} = \frac{T_L}{\frac{1}{2}\rho V^2 A_s}$$

where

T_L is the pre-tension force in the luff-wire.

For the single sail tests both C_{TT} and C_{TL} coefficients are quoted.

5. A non-dimensional elasticity coefficient, defined as the strain in the leech or luff produced by the pre-tension force:

$$\frac{T}{E}$$

where

T is the pre-tension force

E is the force required to produce unit strain, that is the force ideally required to double the length of the luff or leech.

The addition of subscripts T or L to both T and E denotes that the coefficient relates to the trailing edge or leading edge respectively. The values of E were determined experimentally and found to be:

a) 0.78×10^3 lbs/strain for the unsewn leech line

b) 1.86×10^3 lbs/strain for the sewn trailing edge

c) 150×10^3 lbs/strain for the luff wire.

Although quoted to three significant figures, these values are probably accurate to about ±10%.

6. A non-dimensional coefficient based on the elastic properties of the sail cloth and the leech line:

$$\frac{e\bar{c}}{E_T}$$

where

$\bar{c}$ is the mean chord length of the turbine blades defined as $\frac{A_s}{2b}$, A_s being the turbine blade area and b being half the leading edge length of each turbine blade. Substitution gives $\bar{c}$ = 11.2 in. for the double sail and 11.3 in. for the single sail.

e is the force per unit width of the sail for each piece of cloth required to produce unit strain in the sail in the direction of the chord.

In determining e, four small wooden blocks 3 in. long by 3 in. wide and 0.7 in. thick were used. Sand paper was glued on one face of each block to provide a better grip when the blocks were clamped to the sail cloth. A length of 10 in. along the warp of the sail fabric was measured and the wooden blocks were placed cross-wise, two at each end of the measured length and parallel to each other. The sail was sandwiched between the two blocks and then the blocks were clamped tightly. The length of the blocks was taken as the test width of the sail. One pair of blocks was held in a vice while the other pair hung free. Weights were added to it and the extension of the clamped length of the sail was measured by a dial gauge. It was therefore possible to determine e from the measured values of the extension and the weights. The whole procedure was repeated with the test length being measured along the weft direction of the sail fabric. e was found to be 10.5×10^3 lbs/ft. per strain of the sail for both the warp and weft directions of the sail material. This value is accurate to about ±10%.

In relation to the sail blade geometry, the warp of the sail material was along the blade chord and the weft direction was perpendicular to the chord.

7. A non-dimensional density coefficient of the sail cloth given by:

$$\frac{\sigma}{\rho \bar{c}}$$

where

σ is the mass of the cloth per unit area.

σ = 3 oz. per square yard. The average value of $\frac{\sigma}{\rho \bar{c}}$ was 0.30 and did not vary more than ±1.4% during the tests.

8. A non-dimensional porosity coefficient of the sail:

$$\frac{\mu V}{\Delta p \bar{c}}$$

where

v is the normal velocity through the cloth associated with a pressure difference Δp.

The cloth was considered impervious, and as a result this last number is effectively zero.

5.2 Wind Tunnel Interference

Because the tests were performed in an open jet tunnel, wind tunnel interference corrections were only applied for solid blockage. Wake blockage was neglected.

Hence applying solid blockage correction to the tunnel speed;

$$V = V_t(1 + \varepsilon_s)$$

where

V is the tunnel speed after solid blockage correction

V_t is the tunnel speed without solid blockage correction

ε_s is the solid blockage factor.

For an open jet tunnel, Lock (Pankhurst and Holder) [8], gives the following relationship for the solid blockage factor for a body of revolution:

$$\varepsilon_s = \tau\nu\left(\frac{\text{maximum cross-sectional area of body}}{\text{cross-sectional area of tunnel}}\right)^{3/2}$$

where

ν is a factor depending on the shape of the body which has been taken as 1 for a rotating turbine

τ is a factor depending on the shape of the cross-sectional area of the tunnel and the nature of its boundary. For a circular open jet tunnel, $\tau = -0.206$.

After substitution, $\varepsilon_s = -0.014$ and the relationship between corrected and uncorrected tunnel speeds becomes, $V = 0.986\ V_t$. Hence after application of solid blockage interference corrections, the tip speed ratios are increased by 1.4% and the power coefficients are increased by 4.2%. It is interesting to note that a very similar value for solid blockage factor is obtained using Thom's short-form equation for solid blockage for a three-dimensional body of revolution [9].

5.3 Evaluation of Results

The output power from the wind turbine was expressed in the form of a non-dimensional power coefficient given by the conventional relationship,

$$Cp = \frac{P}{\frac{1}{2}\rho AV^3}$$

where

A is the frontal swept area of the turbine

P is the power output from the wind turbine computed from the shaft torque.

Cp was plotted against the tip speed ratio $\lambda = \frac{\Omega R}{V}$ for each test run. The results are shown in Figs. 5 and 6 for the turbine when fitted with double sails, for different Reynolds numbers, pre-tension coefficient, C_{TT} and trailing edge elasticity, T_T/E_T. The letter S denotes tests where the leech line was sewn to the trailing edge. Results of Cp plotted against λ for the single sail are shown in Figs. 10 and 11 for a range of Re, C_{TT}, C_{TL} and trailing and leading edge elasticities T_T/E_T and T_L/E_L respectively.

Due to the relatively high solidity of the wind turbine, the tip speed ratios for positive power were between 0 and 2.5. The tests were performed at Reynolds numbers ranging from 5.6×10^5 to 7.9×10^5.

Free-wheeling results for the double sail are plotted as tip speed ratios, $(\frac{\Omega R}{V})_0$ against the leech pre-tension coefficient, C_{TT} in Fig. 7 for a range of tunnel speeds. Corresponding results for the single sail are shown in Fig. 12.

The double sail was found to be self-starting at low leech-line pre-tension, for values of $C_{TT} < 3$ and trailing edge elasticity, $T_T/E_T > 10^{-2}$ or more. The starting torque was positive for all azimuthal positions when the turbine was self-starting. The starting torque coefficient was given by the expression:

$$C_Q = \frac{Q}{\frac{1}{2}\rho ARV^2}$$

where Q is the average starting torque. C_Q was found to be equal to 0.03.

The single sail was not self-starting but required only a small torque to start it in all cases.

6. DISCUSSION OF RESULTS

6.1 Experimental Results

Due to the very large number of parameters which are required to specify the turbine performance it was not possible to vary one parameter at a time while keeping all the others constant. An approximate analytical theory was therefore developed for sail distortion [10] (Appendix A). The theory gives approximate formulae for the change in blade chord and change in angle of attack due to the sail distortion when under wind load.

The elastic coefficient of the sail material, $\frac{e\bar{c}}{E_T}$, was initially investigated as this had a direct bearing on the choice of sail cloth. The change in blade chord due to the trailing-edge pre-tension was therefore estimated. A small change in chord would indicate that $\frac{e\bar{c}}{E_T}$ had negligible effect on the turbine performance. The analysis (Appendix A) shows that if the applied pre-tension force in the trailing edge is T_T and the extension of the sail in the direction of the chord is δ, then the equilibrium of the double sail blade in the direction of the chord per unit length is:

$$\frac{2\,e\,\delta}{\bar{c}} = \frac{T_T}{s}$$

where

e is the force per unit width of the sail for each piece of cloth required to produce unit strain in the sail in the direction of the chord

$\bar{c}$ is the mean chord of the blade

s is the radius of curvature of the trailing edge of the sail.

From the geometry, $s = \frac{b^2}{8x_T}$.

where

b is the length of half the sail blade

x_T is the trailing edge hollow under pre-tension without wind load.

Substituting for s and re-arranging we get,

$$\frac{\delta}{c} = \frac{E_T}{e\bar{c}} \cdot \frac{T_T}{E_T} \cdot 4\,\frac{\bar{c}}{b} \cdot \frac{x_T}{b}$$

Substituting typical numerical values, $e\bar{c} = 9.80 \times 10^3$ lbs/strain for the present sail cloth, $\frac{\bar{c}}{b} = 0.18$, $\frac{x_T}{b} = 0.03$ and taking an average value of $T_T = 50$ lbs: $\frac{\delta}{c} = 1.10 \times 10^{-4}$ in. and $\delta = 0.001$ in. approximately for the double sail blade. For the single sail $\delta = 0.002$ in. Therefore very little change in chord occurs for both sails under typical leech tensions and it can safely be concluded that $\frac{e\bar{c}}{E_T}$ did not have any significant effect on the turbine performance: it could thus be considered an unimportant parameter. This eliminates the necessity of matching $\frac{e\bar{c}}{E_T}$ for tests where a different sail material would be used. Only a very big decrease in e for the sail material would affect the blade geometry under load and thus the turbine performance.

The effect of the trailing edge pre-tension coefficient, C_{TT} and the trailing edge elasticity, T_T/E_T on the turbine performance can be estimated by considering the change in angle of attack and the change in chord due to sail distortion under wind load. The aerodynamic forces on the trailing edge causing distortion can be resolved into components X per unit span along the chord and towards the leading edge, and Y per unit span perpendicular to the chord in the direction of positive lift. These forces are expressed as non-dimensional coefficients based on the mean chord $\bar{c}$, C_X and C_Y respectively. It is shown in Appendix A, that the change in angle of attack of the sail when loaded by the wind is given approximately by the expression:

$$\varepsilon = \left(\frac{x}{\bar{c} + x_T}\right)\frac{C_Y}{C_X} \qquad \text{(A.14)}$$

where

$\bar{c}$ is the mean chord of the blade

C_X is the trailing edge force coefficient along the chord

C_Y is the trailing edge force coefficient perpendicular to the chord

x is the trailing edge hollow when the blade is aerodynamically loaded.

x_T is the trailing edge hollow after pre-tension without wind load.

The average change in blade chord when the blade is under wind load is given by the relationship:

$$\frac{x - x_T}{b} = \frac{\frac{b}{16x_T}\left(1 + \frac{2}{5}\lambda^2\right)\frac{C_X}{C_{TT}} - i}{\left(1 + \frac{E_T}{T_T}\right)\frac{16}{3}\frac{x_T}{b}} \qquad \text{(A.27)}$$

where

b is half the length of the leading edge of the blade

C_{TT} is the trailing edge pre-tension coefficient

E_T is the force required to produce unit strain in the trailing edge

T_T is the trailing edge pre-tension force

λ is the tip speed ratio.

To evaluate ε and $\frac{x-x_T}{b}$, values of C_X, C_Y and their associated change in camber along the chord are used. These values have been measured by Robert [7] on two dimensional sail aerofoils for a variety of Reynolds numbers and angles of attack. The change in chord may be expressed in a non-dimensional form as $\frac{x-x_T}{\bar{c}}$. For a very taut sail aerofoil, $\frac{x-x_T}{\bar{c}} < 0.01$, C_X ranged from 3 to 5 while $C_Y = 0.5$. For $\frac{x-x_T}{\bar{c}} = 0.03$, $C_X = 2$ and $C_Y = 1$.

If we consider a case where there is negligible change in camber along the chord, equation (A.27) reduces to:

$$\frac{b}{16x_T}\left(1 + \frac{2}{5}\lambda^2\right)\frac{C_X}{C_{TT}} - 1 = 0$$

Therefore the value of C_{TT} for negligible camber change depends on the tip speed ratio squared and the pre-tension trailing edge hollow. Using the values of $C_X = 3$ to 5 and noting that for the turbine blade $\frac{x_T}{b} = 0.03$, the above equation can be solved for a particular tip speed to give the range of C_{TT} which is associated with negligible camber change. Taking $\lambda = 1$, the values of C_{TT} lie between 9 and 15. It is worth noting that by increasing the tip speed ratio λ to say 1.5, the values of C_{TT} for negligible camber change increase to 12 and 20. When the change in camber is negligible, the corresponding change in angle of attack $\varepsilon \doteqdot 1°$ (equation A.14). Therefore with a very small change in angle of attack and negligible change in chord and hence change in camber, the sail blade is effectively rigid. The turbine performance is then independent of C_{TT} and T_T/E_T.

The relative effects of C_{TT} and T_T/E_T on the turbine performance can be compared for a particular change in chord using equation (A.27). By taking the case when the change in chord $\frac{x-x_T}{\bar{c}} = 0.03$ and a tip speed ratio $\lambda = 1$, if $T_T/E_T = 10^{-2}$, the corresponding value of $C_{TT} = 5.4$. On the other hand for the same change in chord and for the same tip speed ratio, increasing T_T/E_T twenty times to 2×10^{-1}, only modestly increases C_{TT} to 5.8. Therefore a relatively small change in C_{TT} is equivalent to a proportionately much larger change in T_T/E_T in its effect on sail distortion and hence turbine performance. If C_{TT} is increased slightly the camber change decreases. The same effect is achieved by a much higher decrease of T_T/E_T. From this analysis therefore C_{TT} is the more important parameter.

Power coefficient results for the double sail are shown in Fig. 5 for a constant Re = 5.6×10^5. The letter S in the legend of the figure indicates tests in which the leech line was sewn to the sail. Sewing the leech line to the sail reduced the elastic coefficient T_T/E_T, of the trailing edge by a factor of 2.4, and this is theoretically equivalent to a very small increase in C_{TT}. At low tip speed ratios, the power coefficient Cp is seen to decrease when C_{TT} and T_T/E_T are increased. At higher tip speed ratios, Cp increases as C_{TT} increases to about 12. For values of C_{TT} between 12 and 15, the trend reverses at higher tip speed ratios until the performance becomes independent of C_{TT} for values of $C_{TT} > 15$ approximately. In Fig. 5, for a $C_{TT} = 11.7$, sewing the leech line results in a reduction of Cp at high tip speed ratios which is contrary to the theory.

Results for the double sail at higher Reynolds numbers (7.1×10^5 to 7.9×10^5) are shown in Fig. 6. For a given Reynolds number, Cp increases at low tip speed ratios when C_{TT} decreases, while at higher tip speed ratios, Cp increases when C_{TT} increases. In this case at $C_{TT} \doteqdot 3.4$ a decrease of T_T/E_T due to sewing the leech line to the sail, produces an effect equivalent to an increase of C_{TT} in agreement with the theory.

Free-wheeling results $(\frac{\Omega R}{V})_0$ for the double sail are plotted against C_{TT} in Fig. 7. The results do not seem to support the conclusion that the performance of the turbine becomes independent of C_{TT} when C_{TT} is large enough and the blades are rigid. To determine if the deviation from the theory is a viscous effect, the free-wheeling results are re-plotted against the Reynolds number in Fig. 8. The numbers beside each data point are the values of C_{TT}. For C_{TT} greater than about 15 all results fall onto a single curve except perhaps at the lower Reynolds numbers where there is scatter which may be attributed to low dynamic pressure. Thus although the tests have been made on a fairly large scale model there are still scale effects. This is seen further in the values of the power coefficient for $C_{TT} > 14$ which are shown in Fig. 9. The power coefficient for three Reynolds numbers is compared and significant improvement in performance with an increase of Reynolds number is clearly observed. The additional results for $Re = 2.2 \times 10^5$ were performed on a smaller wind turbine model of maximum radius R = 5.75 in., height of 16.5 in. and a solidity $\frac{NC_R}{R} = 1.57$. It was tested in a closed wind tunnel with a 3 ft. x 2 ft. working section. Wind tunnel interference corrections were however not applied to the results, and the values of Cp in this case are higher than those which would be expected if wind tunnel interference corrections had been applied.

The turbine when fitted with double sails was self-starting for low values of $C_{TT} < 3$ and $T_T/E_T > 0.01$ or more. From equation (A.27) this was a range of large camber changes. The maximum power coefficient Cp_{max} obtained was 0.16 and occurs when $C_{TT} = 3.3$, $T_T/E_T = 0.02$, $\lambda = 1.25$ and $Re = 7.8 \times 10^5$. The range for positive power output in this case extends to $\lambda = 2$. Increasing C_{TT} increases the range for positive power output but decreases Cp_{max}. Thus in Fig. 6 increasing C_{TT} to about 15, the value of λ for positive Cp increases to 2.6. This increase is accompanied by a reduction of Cp at low λ and a 0.01 reduction in Cp_{max}.

The single sail has two extra criteria of similarity, the leading edge pre-tension coefficient C_{TL} and the leading edge elasticity coefficient T_L/E_L. Power coefficient results for the single sail are shown in Figs. 10 and 11. In Fig. 10, the results are shown for a constant Reynolds number and near constant C_{TT} and T_T/E_T, while the leading edge coefficients C_{TL} and T_L/E_L are varied. Increasing C_{TL} progressively increases the turbine performance and Cp_{max}. However it is noted that the two curves for C_{TL} equal to 41.4 and 24.5 coincide at higher tip speed ratios. This is probably due to the slight difference in C_{TT} for the two curves. The graph for C_{TL} = 24.5 has a slightly higher C_{TT} = 6.3 compared to the value C_{TT} = 5.1 for the curve with C_{TL} = 41.4. As established with the double sail results, an increase of C_{TT} produces an increase in Cp and an increase also of the range for positive power output at higher tip speed ratios.

In Fig. 11, T_L/E_L is kept constant while the Re, C_{TT}, T_T/E_T and C_{TL} are varied. The performance increases with Reynolds numbers except at the higher tip speed ratios where the results tend to coincide. For constant Reynolds number and C_{TL} the results for the single sail at low tip speed ratios behave in a similar manner as those for the double sail. Cp increases at low tip speed ratios as C_{TT} is decreased. The maximum power coefficient for the single sail was 0.16 at λ = 1.23 with C_{TT} = 3.1 and T_T/E_T = 0.02 at Re = 7.1 x 10^5. Maximum range for positive Cp was λ = 1.95 when C_{TT} = 12.7.

Free-wheeling results for the single sail are shown in Fig. 12. The results do not resemble those obtained for the double sail blades and appear to be relatively insensitive to both C_{TT} and Re. The latter may be due to the comparative insensitivity of aerofoils with sharp leading edges at small incidence to changes in Reynolds number for Reynolds numbers in the range 10^4 to 10^5. At small incidences, sharp leading edges have a fixed separation point and this does not change irrespective of changes in Reynolds numbers whereas the laminar separation point on conventional aerofoils tends to vary with Reynolds number over this range.

The power coefficient for both the single sail and double sail blades were of comparable magnitude. The range of positive power output was however smaller with the single sail than with the double sails. Maximum power coefficient was obtained with almost the same values of C_{TT} and λ, for both types of blades. Whereas the double sail was self-starting for all azimuthal positions for low values of C_{TT} (less than 3), the single sail was not self-starting for any values of C_{TT}. However it might self-start in a field application where the wind is turbulent and of a scale which significantly varies the wind direction.

6.2. Comparison of Experimental Results with Simulated Results

A theory for vertical-axis wind turbines has been proposed by Templin [4]. The induced velocity through the turbine, termed the disc velocity, is related to the wind turbine drag using one dimensional actuator disc theory. Using Blade Element theory, the drag and torque of a blade element of the turbine can be determined when the local blade characteristics are known. For given values of the rotational speed and ambient wind speed, the turbine torque and power output are evaluated as follows:

1) A disc velocity, that is wind velocity at the turbine is assumed.
2) The turbine drag is then found by integrating the contributions of each blade element over the full height of the turbine and over one complete revolution.

3) The disc velocity associated with this drag is calculated using Actuator Disc Theory [11].

4) The new value of the disc velocity is then used for a repeat calculation and the iteration is continued until the changes in disc velocity become small enough to be unimportant. The output torque and power are then computed.

5) The procedure is then repeated for a different rotational speed.

The computer program used in the simulation of the turbine performance was written by Robert [7] and only minor changes were required to take into account the characteristics of the wind turbine tested. The data used in the program were Robert's measurements of thrust and normal force coefficient for a two dimensional aerofoil for various angles of attack and Reynolds numbers.

From Actuator Disc Theory, the disc velocity can only have a value lying between the ambient wind speed and half the ambient wind speed. For lower values of the disc velocity, the wake velocity becomes negative and the theory fails. Turbines with high solidity operate more in this low range of disc velocity. In applying Templin's method for turbines with high solidity, the relationship between the disc velocity and the turbine drag has to be extended empirically. Three extensions are presented in this text.

In Fig. 13, the drag coefficient is plotted against the disc velocity ratio,

$$\frac{V_D}{V}$$

where

V_D is the induced disc velocity

V is the ambient wind speed.

Curve No. 1 in the figure shows the plot according to Actuator Disc Theory, and in the range $0 < \frac{V_D}{V} < 0.5$, the theory does not work. Curve No. 2 shows an empirical representation by Robert [7] to cover the range $1 > \frac{V_D}{V} > 0.5$. The disc velocity ratio is expressed in the form:

$$\frac{V_D}{V} = \left[1 - \frac{C_D}{C_{D_{PL}}}\right]^y$$

where

C_D is the drag coefficient

$C_{D_{PL}}$ is the drag coefficient of a fully solid wind turbine

V is the ambient wind speed

V_D is the induced disc velocity

y is an exponent

By matching the same optimum conditions as stipulated by the Actuator Disc Theory, $C_{D_{PL}}$ and y were determined. Robert's final expression was:

$$\frac{V_D}{V} = \left(1 - \frac{C_D}{1.1147}\right)^{0.254}$$

From this relationship, C_D clearly cannot exceed 1.1147. When this relationship was used in the program, it was found that for the solidity of the turbine tested, the value of C_D exceeded 1.1147 for $\lambda > 1$. Alternative expressions were therefore tried. Curve No. 3 in Fig. 13 is based on an expression where the disc velocity ratio is expressed in the form:

$$\frac{V_D}{V} = 1 - \left(\frac{C_D}{C_{D_{PL}}}\right)^n$$

where

C_D is the drag coefficient

$C_{D_{PL}}$ is the drag coefficient of a fully solid wind turbine

n is an exponent

V is the ambient wind velocity

V_D is the induced disc velocity.

By assuming again the same optimum values as given by the Actuator Disc theory, the exponents $C_{D_{PL}}$ and n were calculated. The final expression is:

$$\frac{V_D}{V} = 1 - \left(\frac{C_D}{1.539}\right)^2$$

Curve No. 4 in Fig. 13 is an empirical expression in rough agreement with data collected by Stoddard [12] for helicopter and wind turbine rotors from references [13, 14].

Experimental results for the double sail blades with $C_{TT} > 14$ are compared with theoretical results based on the three extensions to the Actuator Disc theory for Reynolds numbers 5.6×10^5 and 7.1×10^5 in Fig. 14. By comparing experimental values with $C_{TT} > 14$, distortion of the sail blades did not have to be considered: two dimensional results for the taut condition were used.

The results show very little difference between the three theories up to a tip speed ratio $\lambda = 1$, which is equal to a disc velocity ratio $\frac{V_D}{V} = 0.5$, and further the theories are in good agreement with the experimental values in this range. As λ increases above 1, $\frac{V_D}{V}$ decreases below 0.5 falling in the region in which Actuator Disc theory fails, and the experimental and theoretical results show marked deviation. Stoddard [12] refers to this region in which Actuator Disc theory breaks down as the "turbulent wake" region. It is characterized by high turbulence, wake expansion and increased drag. The variation between theory and experimental results is no doubt broadly due to the one dimensional approach used in the theory.

There are also differences between the three pairs of theoretical results (Fig. 14). The results based on Robert's expression could only give positive power output up to $\lambda = 1$ at which point the turbine drag coefficient, $C_D = 1.1147$, was the maximum allowable by the expression. A comparison of the remaining two expressions shows that from Fig. 13 for a given C_D value above 1.2, the disc velocity is higher for curve No. 4 than for curve No. 3. As a result the power coefficient based on curve No. 4 is higher than that based on curve No. 3 (Fig. 14). The difference between experimental and theoretical results for $\lambda > 1$ is probably due to wake effects. The forward blade reduces the dynamic pressure over the rear blade. In Fig. 14, at higher tip speed ratios, the trend between experimental and theoretical results reverses. Experimental values of Cp are higher than the theoretical results at large λ; C_D is then very high and perhaps the empirical expressions used in the theory become unrealistic.

7. DISCUSSION OF THE FACTORS GOVERNING THE DESIGN

By designing the wind turbine with a high solidity, $\frac{Nc_R}{R} = 1.4$, the wind turbine's tip speed ratios were low and as a result the turbine operated over the complete range of angles of attack, unlike the small range typical with solid blades operating at higher tip speed ratios. Thus the design was less efficient and the measured values of Cp were about half of those normally associated with the Darrieus turbines with solid blades. For example the National Research Council's 14 ft. diameter Vertical Axis wind turbine with solid blades gave a maximum Cp of 0.37 [15].

Notwithstanding the low values of Cp, operation of the turbine at low tip speed ratios has the following advantages:

1) Excessive loads on the blades are avoided.
2) Self-starting may be achieved.
3) Vibrations originating from dynamic imbalance are reduced. In this case the wind turbine was only balanced statically and not dynamically.
4) The power loss associated with the adverse torque of the central supporting disc was reduced.
5) For the case of the double sail blades, the centrifugal stresses in the leading edge dowels were reduced.

The first critical whirling speed for the wind turbine was analytically determined by summing the separate effects of a concentrated mass representing the central disc and a distributed mass representing the wind turbine shaft. Since the turbine bearings were self aligning pin jointed ends were assumed. Dunkerley's method [16] was used to calculate the resultant critical speed, as shown:

$$\frac{1}{\Omega_c^2} = \frac{1}{\Omega_1^2} + \frac{1}{\Omega_2^2}$$

where

Ω_c is the resultant critical speed according to Dunkerley

Ω_1 is the first critical speed for the shaft alone

Ω_2 is the first critical speed due to the central disc mass ignoring the mass of the shaft.

Substituting relevant values for Ω_1 and Ω_2 [17], above we get:

$$\frac{1}{\Omega_c^2} = \frac{m L^4}{96 E_Y I} + \frac{M_c L^3}{48 E_Y I}$$

where

E_Y is the Young's Modulus of the shaft

I is the moment of inertia of the cross-section of the shaft about a diameter

L is the length of the shaft between the bearings

m is the distributed mass of the shaft per unit length

M_c is the additional mass concentrated at the centre of the shaft.

Substitution of numerical values gave Ω_c = 340 rpm. This calculated value for the whirling speed is probably too low as no allowance has been made for the stiffening effect of the frame due to the leading edge dowels or due to the taut wire in the case of the single sail. The turbine was run at speeds of 200 rpm or less, that is well below the calculated critical speed, and the shaft did not whirl.

A numerical analysis of the loading of the leading edge dowels when the turbine is fitted with double sails, showed that the maximum stresses in the dowels due to centrifugal loads were proportional to:

$$\frac{b^2}{Rd}\ \rho_d\ \lambda^2\ V^2$$

where

b is the length of the leading edge dowel

d is its diameter

ρ_d is its density.

For a given turbine geometry, $\frac{b^2}{Rd}$ is a constant. Therefore for a specific wind speed V, the maximum stresses are proportional to the density of the dowel and the tip speed ratio λ squared. To reduce these stresses entails a reduction in tip speed ratio and thus the advantages of running the turbine at low λ is apparent. Furthermore as a determinant of failure the significant parameter is $\rho_d/\sigma y$, where σy is the ultimate stress. Wood is therefore as good a choice as any other material.

The central disc provided support for the leading edge dowels or wires and the trailing edge leech lines. It was made from a plywood disc of 6 ft. diameter and was lightened with cut-outs in the lightly stressed areas. The loss of power for a rotating disc of similar form to the one used in the present design, is:

$$\Delta Cp = \lambda^3 \frac{R^2}{A} \cdot C_M$$

where C_M is the moment coefficient which is a function of the rotational Reynolds number, $\frac{\rho R^2 \Omega}{\mu}$ [18]. Assuming a wind speed of 22 ft/sec and a $\lambda = 1$, for the tests $\frac{\rho R^2 \Omega}{\mu} = 4.2 \times 10^5$, and from reference [18], $C_M = 0.01$. Hence $\Delta Cp = 0.003$.

A supporting structure consisting of a solid disc therefore results in an acceptable loss of power. However such an arrangement would probably be impractical due to structural reasons in turbines producing about 1kW at 15 mph (22 ft/sec) which would be about three times the size of the model tested.

As a matter of comparison, an estimate of the power absorbed by N struts of constant chord c and drag coefficient C_D is given in Appendix B. The loss of power in terms of the power coefficient is given by the expression:

$$\Delta Cp = \lambda \frac{C_D}{2}\left(\frac{Nc}{R}\right)\left(\frac{R^2}{A}\right) \left[\frac{15}{16} \frac{1}{\lambda^2} + \left\{\left(1 - \frac{1}{\lambda^2}\right)\left(1 + \frac{\lambda^2}{2}\right)\right\}\right] \quad (B.13)$$

where the last term in parentheses applies only when $\lambda > 1$. For the present design, $N = 3$, $R \doteq 3$, $A = 2\sqrt{3}\, R^2$, $c = 1.5$ ft. and taking $\lambda = 1$;

$$\Delta Cp = 0.20\, C_D.$$

Therefore to limit the loss of power to about $\Delta Cp = 0.005$, the drag coefficient of the individual struts must be less than 0.025. Thus the struts must be well streamlined.

From equation (B.13), it can be seen that at high tip speed ratios, the loss of power becomes proportional to λ^3 and may therefore become very large. Operating at low λ therefore reduces the power loss associated with the drag of the central structure.

8. CONCLUSIONS

A 9 ft. high, 6 ft. diameter vertical axis wind turbine has been tested using two types of sail blade. Due to its relatively high solidity of 1.4, the turbine operates at low tip speed ratios and produces comparatively low power output vis a vis the low solidity Darrieus machines with solid aerofoil blades which operate at tip speed ratios of about 6.

For low trailing edge pre-tension coefficient $C_{TT} < 3$ and stiffness $T_T/E_T > 0.1$, the turbine when fitted with double sail blades is found to be self-starting with a starting torque coefficient $C_Q = 0.03$. Maximum power coefficient, $Cp_{max} = 0.16$ was obtained when $C_{TT} = 3.3$, $T_T/E_T = 0.02$, at a tip speed ratio, $\lambda = 1.35$ and at a Reynolds number, $Re = 7.8 \times 10^5$. Positive power output is obtained up to $\lambda = 2.0$ and by increasing C_{TT} to 15, the positive power output range may be increased to $\lambda = 2.6$ at the expense of a slight reduction of Cp_{max}. A theoretical analysis of blade distortion for the double sail when aerodynamically loaded has been presented and found to compare fairly well with the experimental observations. From the theory it has been shown that the turbine performance is independent of the elastic properties of the sail cloth, $\frac{e\bar{c}}{E_T}$ for the sail used in the tests. It has also been shown that the turbine performance becomes independent of C_{TT} and T_T/E_T when $C_{TT} > 15$. Theoretical results based on computer simulation of blade element theory have been compared with experiments for $C_{TT} > 14$. Agreement was found to be satisfactory at low λ, but for values of $\lambda > 1\frac{1}{2}$, the Actuator Disc theory which was used to give the inflow factor (disc velocity ratio) becomes inaccurate. Empirical modifications to extend the range of the theory have been only partially successful.

When fitted with single sail blades, the turbine was not self-starting. The maximum power coefficient obtained in this case was 0.16 at Re = 7.1×10^5 when the trailing edge pre-tension coefficient $C_{TL} > 25$, tip speed ratio $\lambda = 1.23$ and the trailing edge stiffness $T_T/E_T = 0.02$. With the single sail blades, positive power output is obtained up to $\lambda = 1.9$. The single sail performance is again independent of C_{TT} when $C_{TT} > 15$.

The turbine performance, especially when fitted with double sail blades would likely increase with an increase in scale. For a larger turbine it would probably be undesirable to use a central disc to support the blades; instead separate arms might be used but these would have to be well streamlined to avoid unacceptable loss of power, or even removed completely.

It is possible to use wood for most parts of the wind turbine and some other type of cloth such as cotton for the blades. In such a case the material should be made impervious, resistant against decay and also light enough to easily change camber during rotation. However it would be unattractive to replace the metal bearings with wooden bearings. This is particularly true for the lower bearing which supports the weight of the turbine and therefore would have a higher frictional torque. The wind turbine should be statically balanced, but dynamic balancing is probably unnecessary.

The critical whirling speed of the turbine should be checked and the design modified to operate below the critical speed.

Although producing comparatively low power coefficients, the vertical axis sail wind turbine may be useful when power outputs of about 1 kW are required, especially in the developing countries of the world.

Finally one can summarize the advantages of a sail wind turbine producing a power output of about 1 kW when compared to a similar size with solid blades:

Advantages

1) It is cheaper and requires less sophisticated technology to build it. It can therefore be ideal for use in developing nations where the level of technology is low and the cost can be reduced by using local materials.
2) It can be self-starting and gives higher torques at low angular velocities.
3) It may be furled in high winds, which eliminates the use of spoilers typical with designs using solid aerofoil blades.

Disadvantages

1) It is less efficient by a factor of over two.
2) It is less durable, as the sails are liable to be affected by weather conditions and possibly ultra violet radiation after some time.
3) It requires a central supporting structure which results in some loss of power.

REFERENCES

[1] N.G. CALVERT, 1975 'The Mono-Kairos Windmills of Lasithi'. Reprint from the Annual of the British School of Archaeology at Athens, Volume 70.

[2] B.G. NEWMAN, 1974 'Measurements on a Savonius Rotor with Variable Gap'. Paper presented at a Symposium on Wind Energy, Achievements and Potential, held at the University of Sherbrooke.

[3] P. SOUTH and R.S. RANGI, 1971 'Preliminary Tests of a High Speed Vertical-Axis Windmill Model'. National Research Council of Canada, NRC NAE LTR-LA-74.

[4] R.J. TEMPLIN, 1974 'Aerodynamic Performance theory for the NRC Vertical-Axis Wind Turbine'. National Research Council of Canada, NRC NAE LTR-LA-160.

[5] R.J. TEMPLIN and P. SOUTH, 1971 'Some Design Aspects of High-Speed Vertical-Axis Wind Turbines'. National Research Council, Canada. Paper No. C1 presented to the International Symposium on Wind Energy Systems held at St. John's College, Cambridge, England.

[6] M.E. PARKES and F.J.M. van de LAAK, 1976 'Wind Power Installations for Water Pumping in Developing Countries'. Paper No. F3 presented to the International Symposium on Wind Energy Systems held at St. John's College, Cambridge, England.

[7] J. ROBERT, 1977 'Sail Aerofoil Applied to a Vertical-Axis Wind Turbine'. M.Eng. Thesis, Department of Mechanical Engineering, McGill University.

[8] R.C. PANKHURST and D.W. HOLDER, 1952 'Wind Tunnel Technique', Sir Isaac Pitman and Sons, Ltd., London.

[9] ALAN POPE, 1954 'Wind Tunnel Testing', Second Edition, John Wiley and Sons, Inc., New York.

[10] B.G. NEWMAN and T.M. NGABO 'The Design and Testing of a Vertical-Axis Wind Turbine Using Sails'. Submitted for publication, 1978.

[11] H. GLAUERT, 1948 'The Elements of Aerofoil and Airscrew Theory', Second Edition, Cambridge University Press.

[12] F.S. STODDARD, 1977 'Momentum Theory and Flow States for Windmills'. Paper printed in the Wind Technology Journal, Vol. 1, No. 1, published by the American Wind Energy Association.

[13] A. GESSOW and G.C. MYERS, 1952 'Aerodynamics of the Helicopter', Frederick Ungar Publishing.

[14] S.N. WALKER, 1976 'Performance and Optimum Design Analysis/Computation for Propeller Type Wind Turbine'. Ph.D. Thesis, Mechanical Engineering, Oregon State University.

[15] P. SOUTH and R.S. RANGI, 1972 'A Wind Tunnel Investigation of a 14 ft. Diameter Vertical-Axis Windmill'. National Research Council of Canada, NRC NAE LTR-LA-105.

[16] WILLIAM T. THOMSON, 1965 'Vibration Theory and Applications', Second Impression, George Allen and Unwin Ltd., London.

[17] M.F. POTTS, 1971 'Design of Machine Elements', Fourth Edition, Prentice-Hall, Inc., Englewood Cliffs, N.J.

[18] H. SCHLICHTING, 1968 'Boundary-Layer Theory', Sixth Edition, McGraw-Hill Book Company.

[19] R.E. CHILCOTT, 1967 'Notes on the Development of the Brace Airscrew Windmill as a Prime Mover'. Brace Research Institute Technical Report No. T37.

LIST OF FIGURES

Figure 6 Power coefficient plotted against tip speed ratio for the double sail blades at Re = 7.1×10^5. S indicates a sewn leech line.

Figure 7 Free-wheeling tip speed ratios (when Cp = 0) plotted against the leech-line pre-tension coefficient for the double sail blades. S indicates a sewn leech line.

Figure 8 Replot of Fig. 7 showing the variation of free-wheeling tip speed ratios with Reynolds numbers for the double sail blades. The values of C_{TT} are shown for each data point.

Figure 9 Power coefficient plotted against tip speed ratios for the double sail blades for values of $C_{TT} > 14$, indicating the effect of varying the Reynolds number.

Figure 10 Power coefficient plotted against tip speed ratios for the single sail blade, showing the effect of increasing the leading edge pre-tension coefficient.

Figure 11 Power coefficient plotted against tip speed ratio for the single sail blade, showing the effect of varying the trailing edge pre-tension coefficient and the Reynolds number.

Figure 12 Free-wheeling tip speed ratios (when Cp = 0) plotted against the trailing edge pre-tension coefficient for the single sail blades.

FIGURES

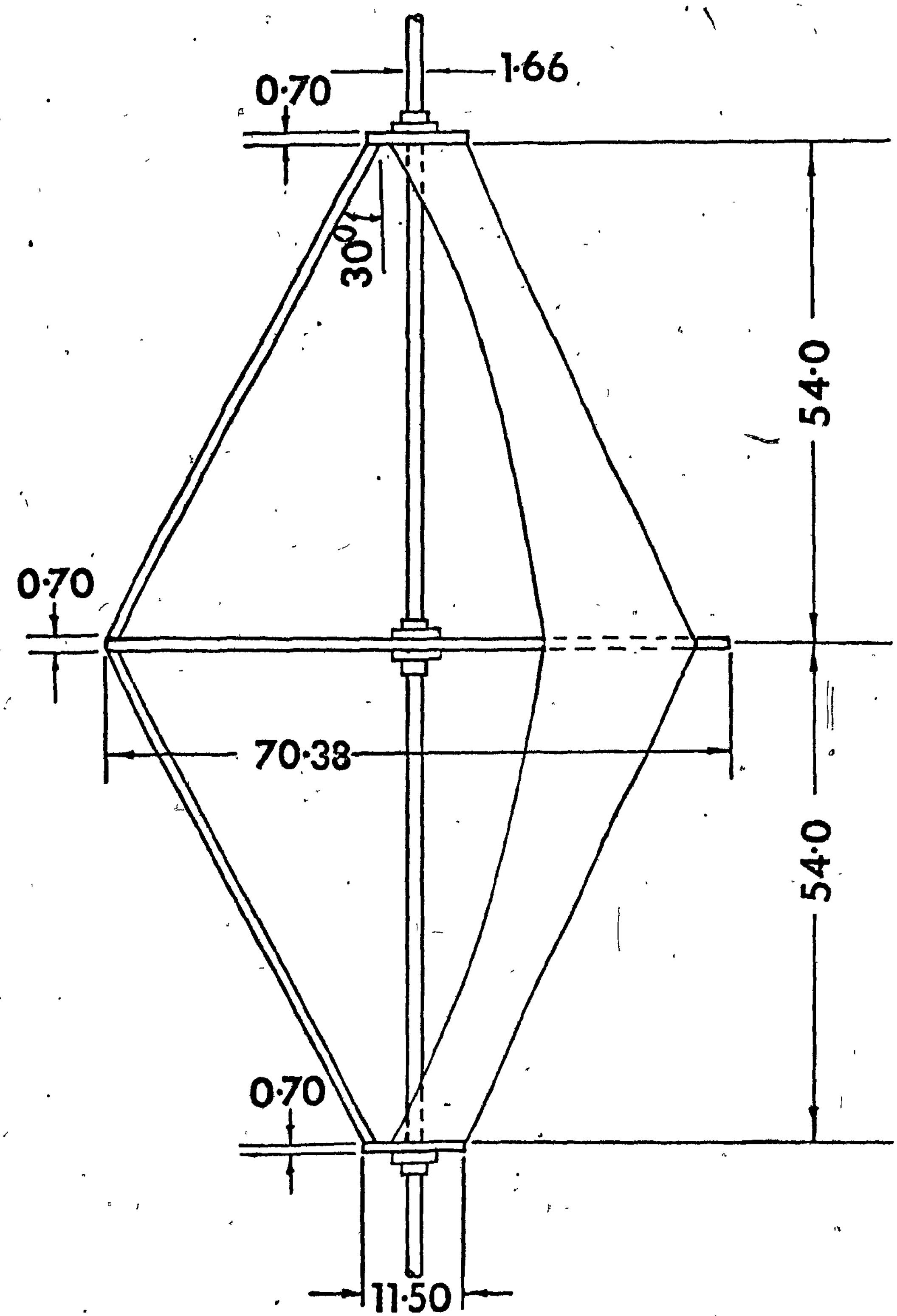

Figure 1   Side view of the wind turbine with the principal dimensions in inches.

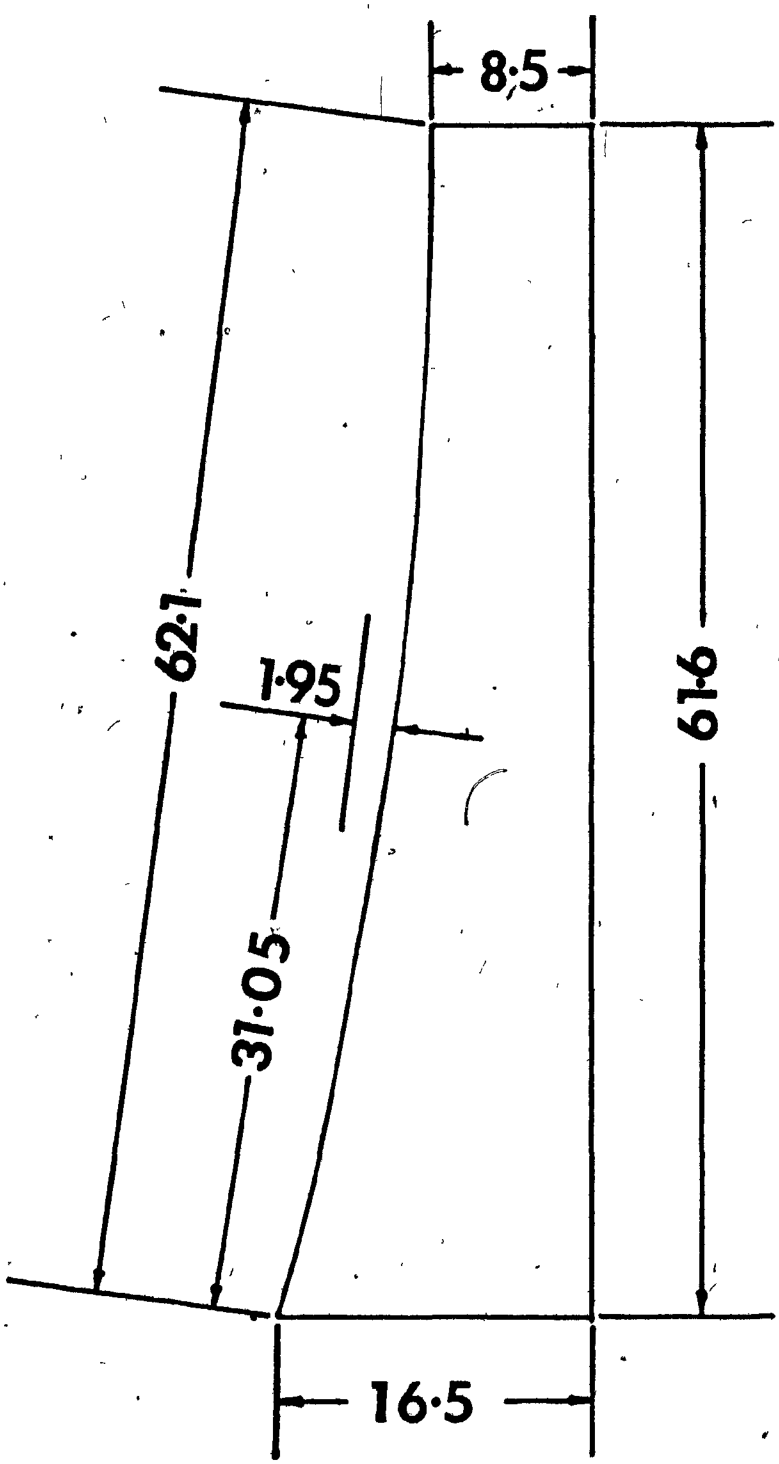

Figure 2 Plan view of half sail blade with the average dimensions for the double and single sails in inches.

WIND TURBINE FITTED WITH DOUBLE SAIL BLADES

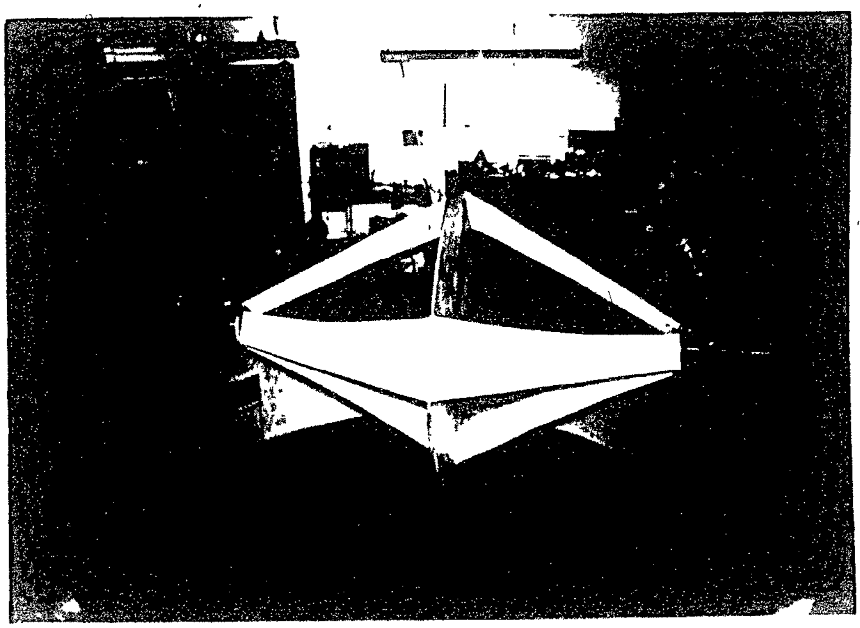

Figure 3a: Wind turbine with double sail blades mounted horizontally on arms in the vertical open jet wind tunnel.

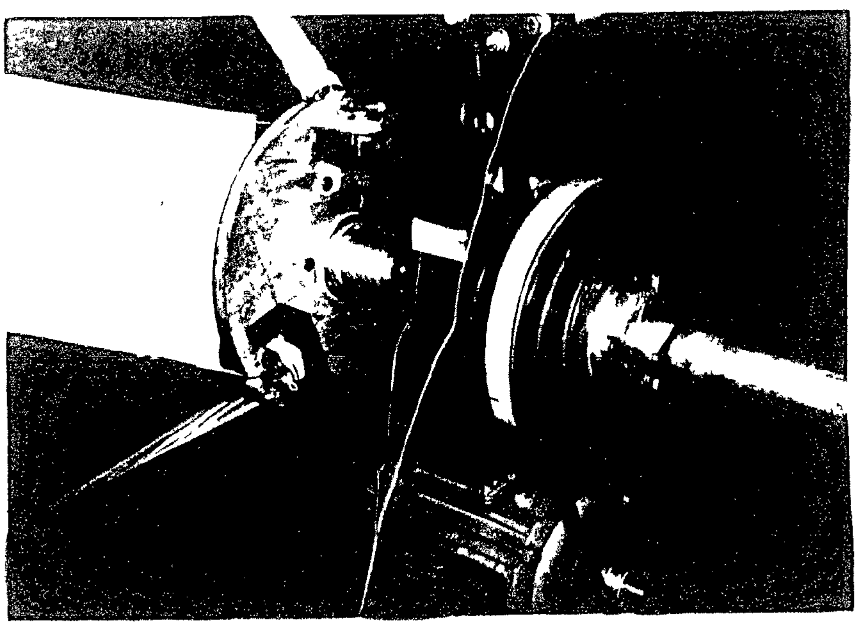

Figure 3b: Close-up of the end disc showing the ratchet mounted drums for tensioning the leech line, the small disc used for measuring the turbine angular velocity, the scale for measuring the torque mounted on the pulley, the vee-belt and the motor generator.

WIND TURBINE FITTED WITH SINGLE SAIL BLADES

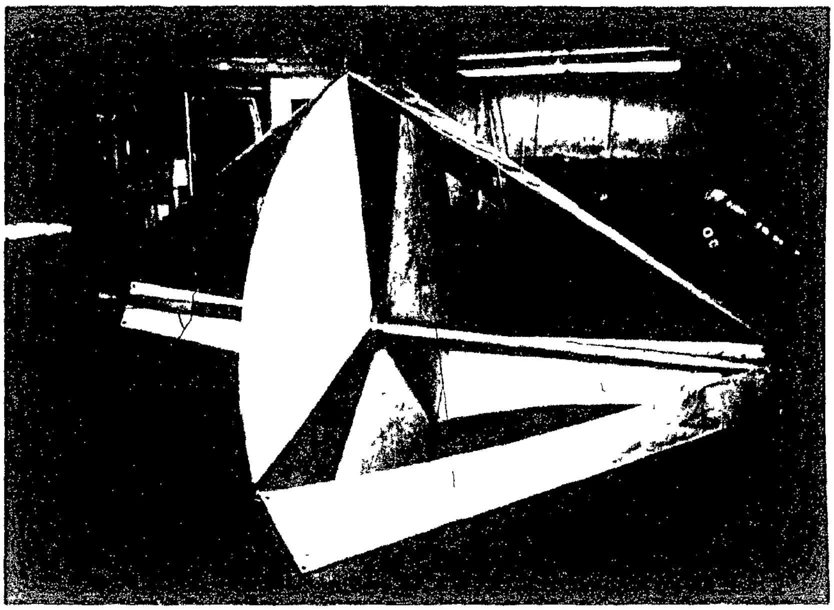

Figure 4a: Wind turbine with single sail blades mounted horizontally on arms in the wind tunnel.

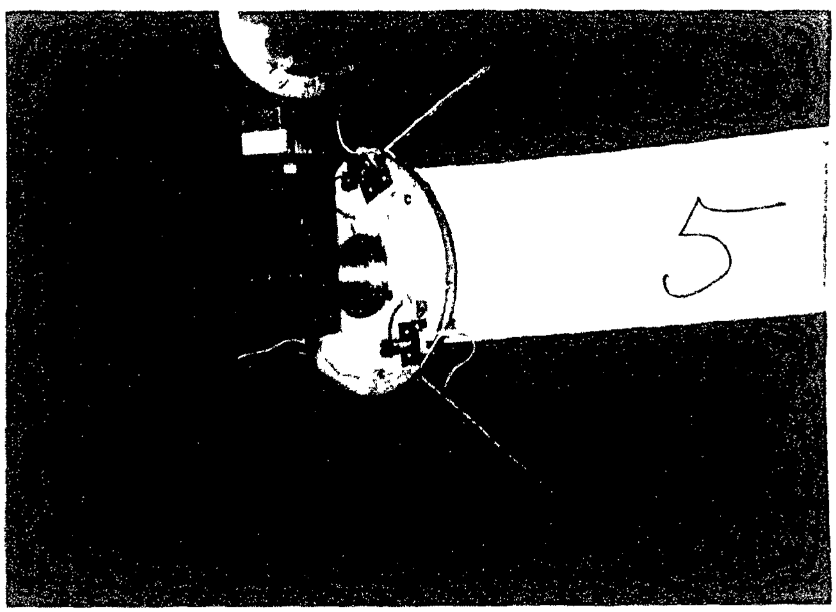

Figure 4b: Close-up of the end disc showing the screw mechanism for tensioning the luff wire.

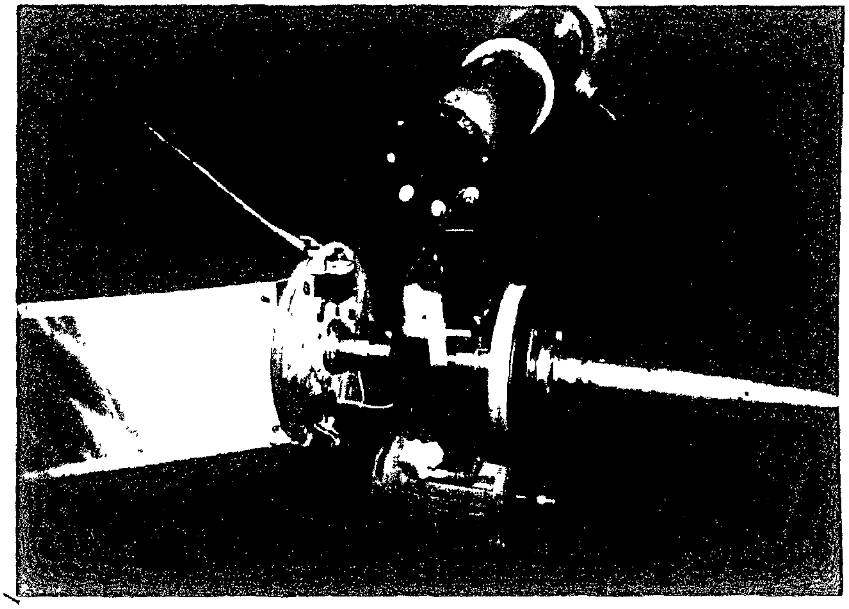

Figure 4c: Close-up of the other end disc showing the ratchet mounted drums for tensioning the leech line, the small disc for measuring the turbine angular velocity, the scale for measuring the torque mounted on the pulley, the vee-belt and the motor generator.

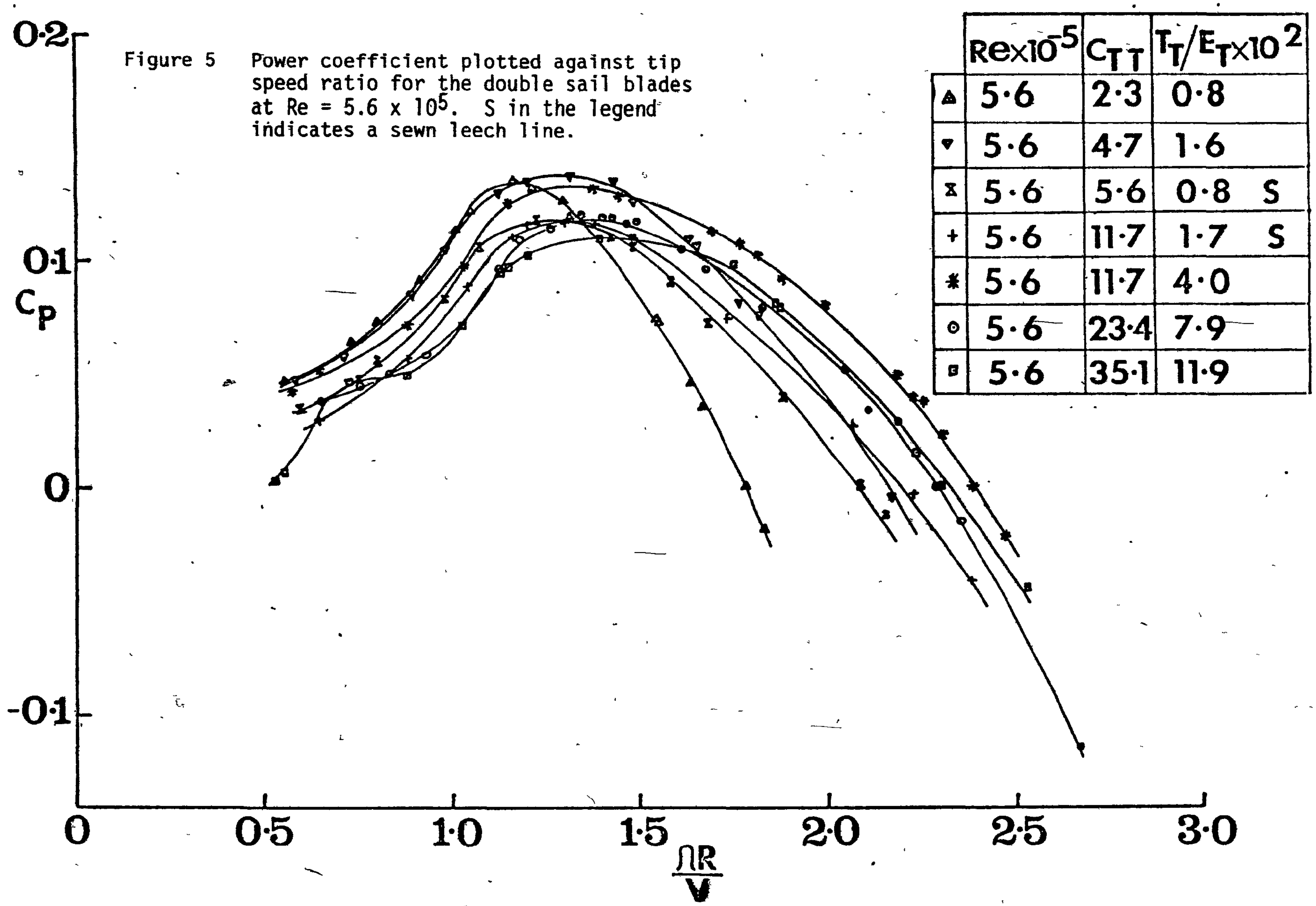

Figure 5 Power coefficient plotted against tip speed ratio for the double sail blades at Re = 5.6 x 10^5. S in the legend indicates a sewn leech line.

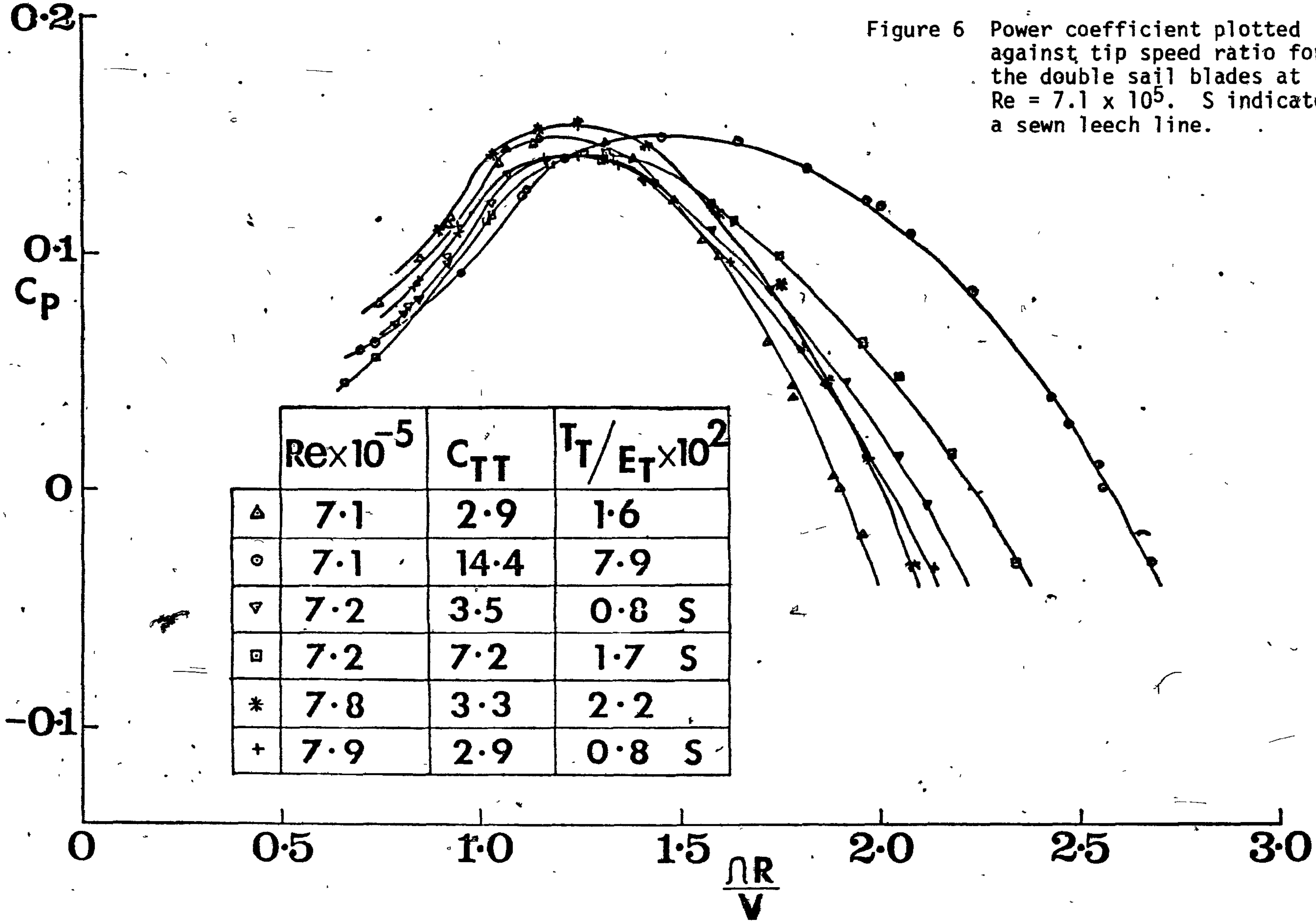

	$Re \times 10^{-5}$	C_{TT}	$T_T/E_T \times 10^2$
△	7·1	2·9	1·6
○	7·1	14·4	7·9
▽	7·2	3·5	0·8 S
□	7·2	7·2	1·7 S
*	7·8	3·3	2·2
+	7·9	2·9	0·8 S

Figure 6 Power coefficient plotted against tip speed ratio for the double sail blades at Re = 7.1 x 10^5. S indicates a sewn leech line.

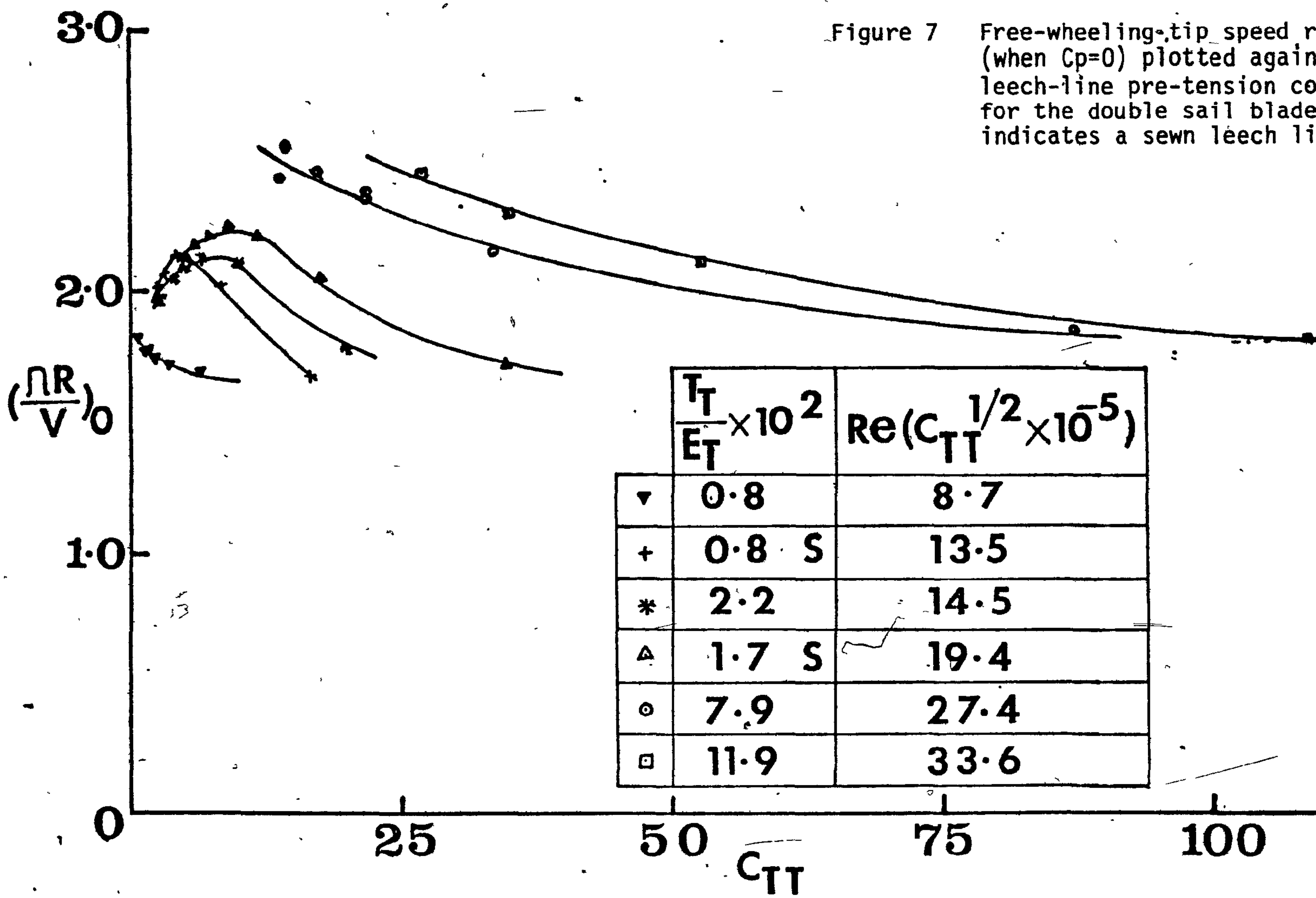

Figure 7 Free-wheeling tip speed ratios (when Cp=0) plotted against the leech-line pre-tension coefficient for the double sail blades. S indicates a sewn leech line.

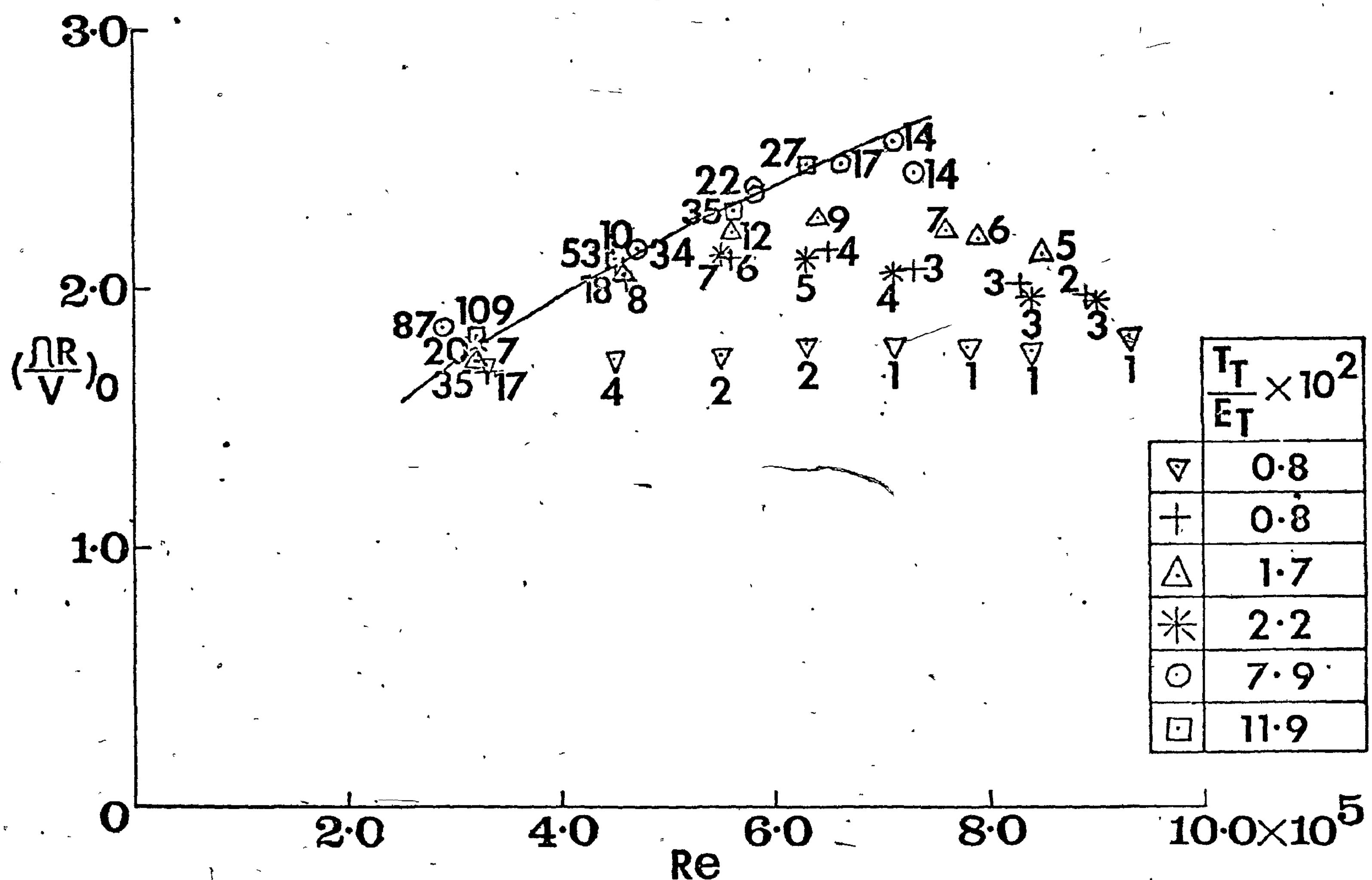

Figure 8 Replot of Fig. 7 showing the variation of free-wheeling tip speed ratios with Reynolds numbers for the double sail blades. The value of C_{TT} is shown for each data point.

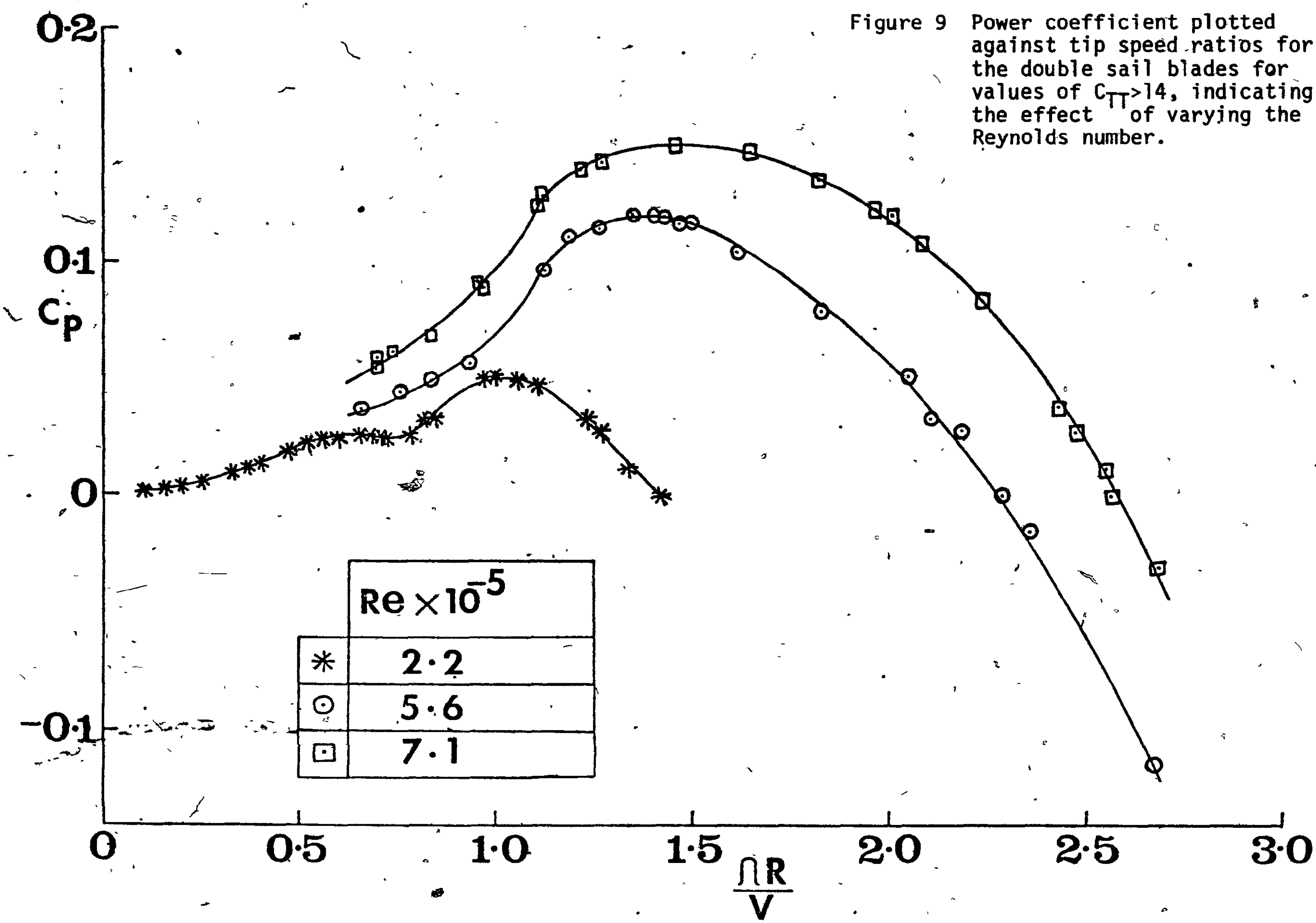

Figure 9 Power coefficient plotted against tip speed ratios for the double sail blades for values of $C_{TT}>14$, indicating the effect of varying the Reynolds number.

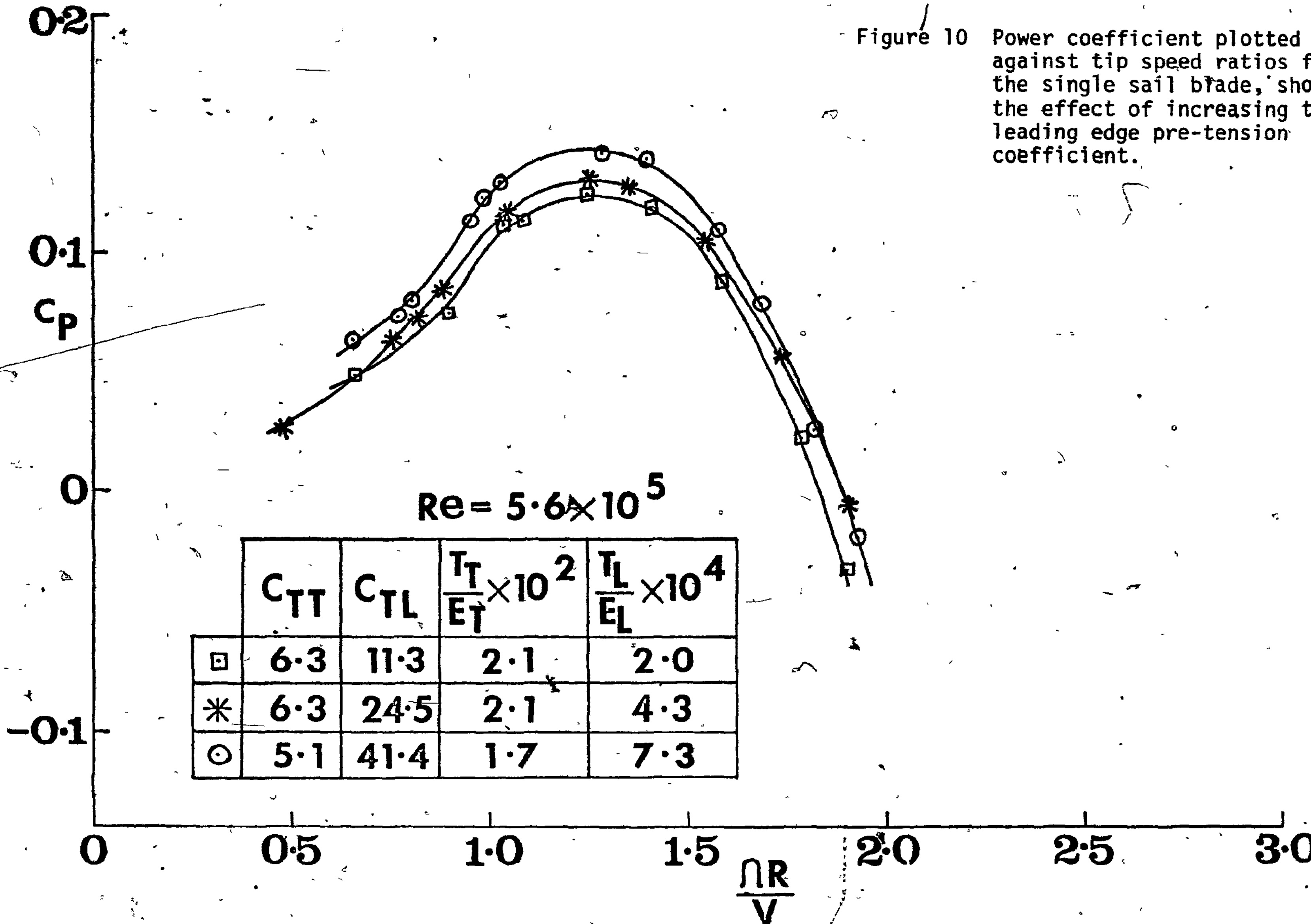

Figure 10 Power coefficient plotted against tip speed ratios for the single sail blade, showing the effect of increasing the leading edge pre-tension coefficient.

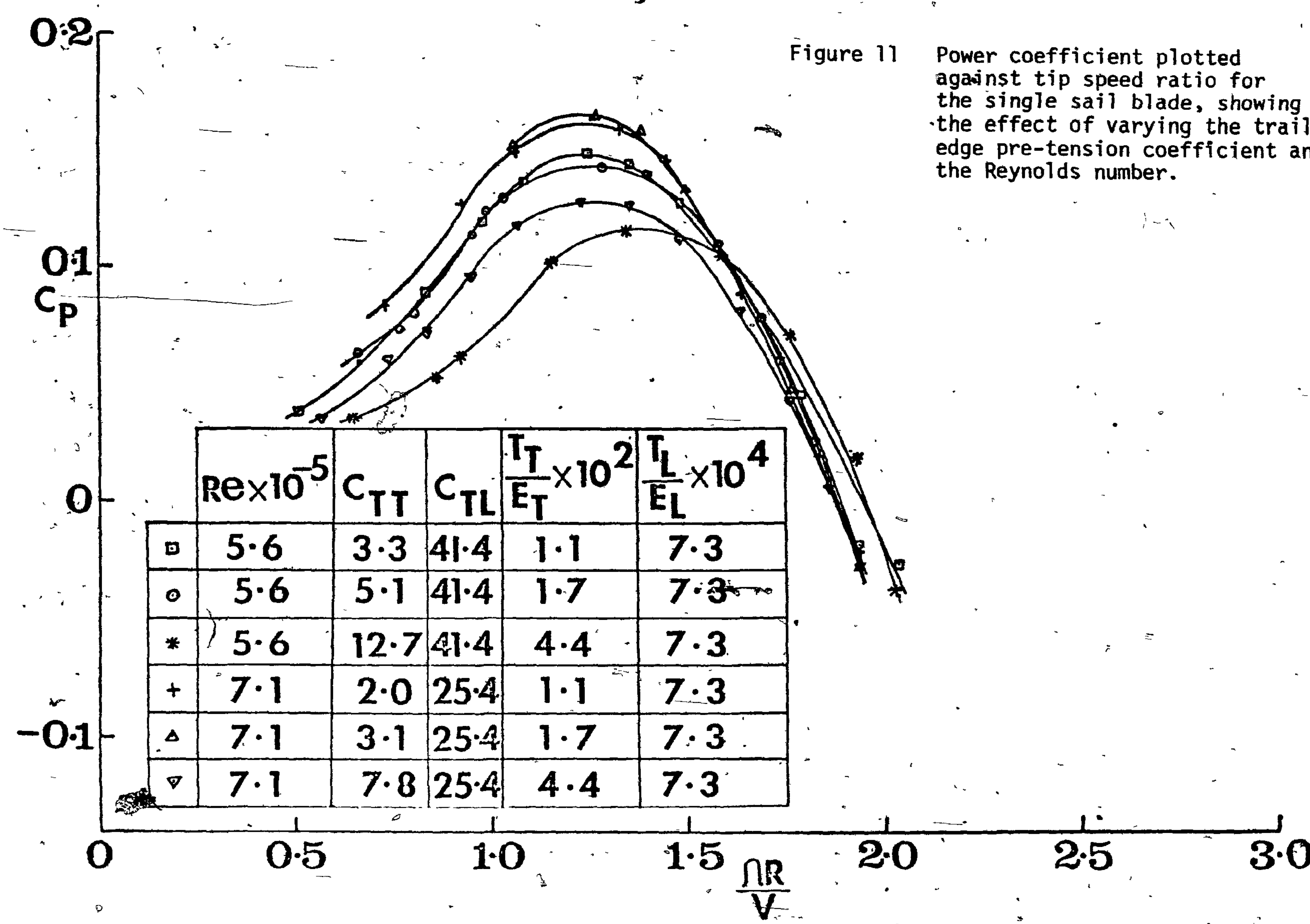

	$Re \times 10^{-5}$	C_{TT}	C_{TL}	$\frac{T_T}{E_T} \times 10^2$	$\frac{T_L}{E_L} \times 10^4$
□	5·6	3·3	41·4	1·1	7·3
○	5·6	5·1	41·4	1·7	7·3
*	5·6	12·7	41·4	4·4	7·3
+	7·1	2·0	25·4	1·1	7·3
△	7·1	3·1	25·4	1·7	7·3
▽	7·1	7·8	25·4	4·4	7·3

Figure 11 Power coefficient plotted against tip speed ratio for the single sail blade, showing the effect of varying the trailing edge pre-tension coefficient and the Reynolds number.

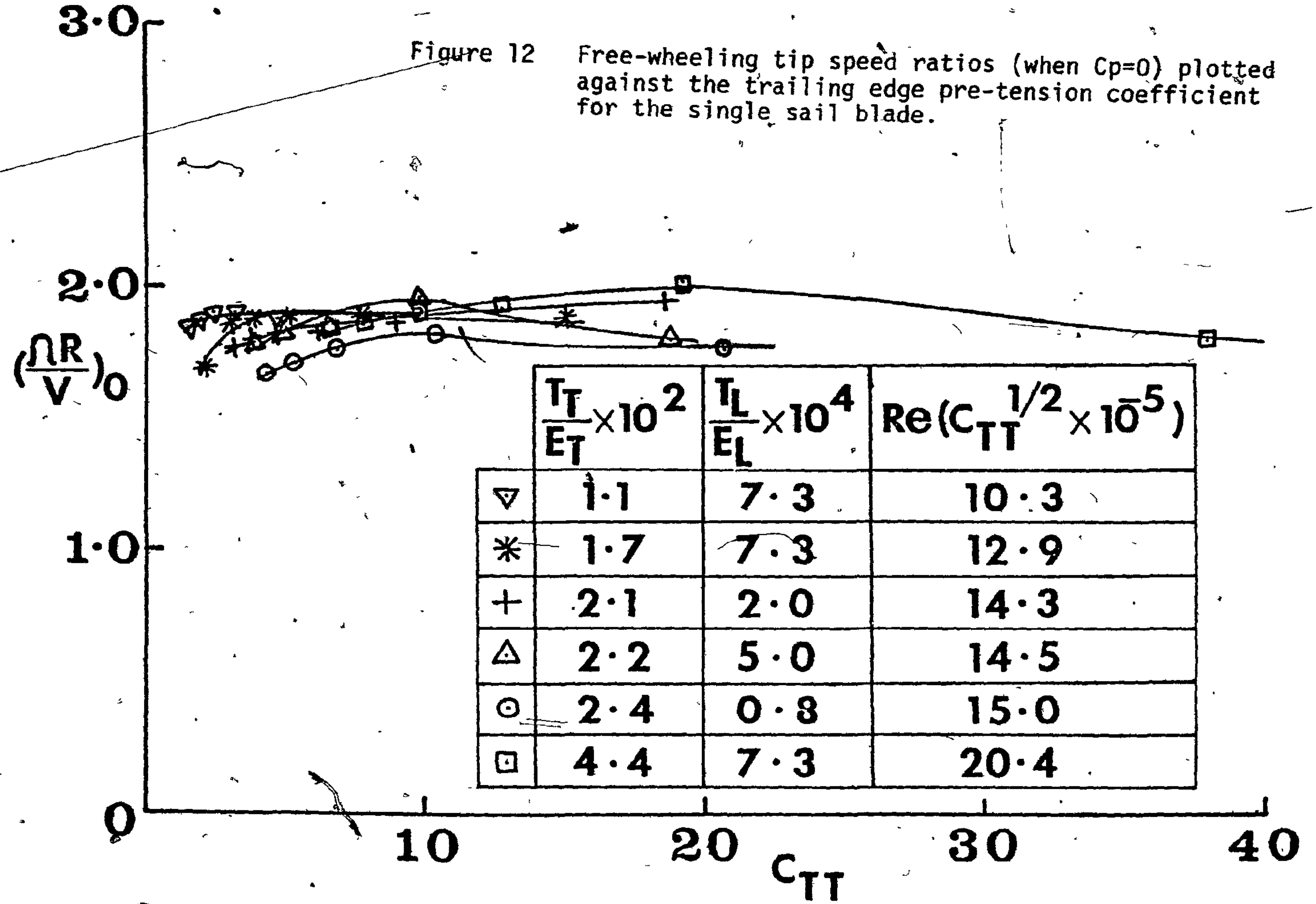

Figure 12 Free-wheeling tip speed ratios (when Cp=0) plotted against the trailing edge pre-tension coefficient for the single sail blade.

	$\frac{T_T}{E_T}\times10^2$	$\frac{T_L}{E_L}\times10^4$	$Re(C_{TT}^{1/2}\times10^{-5})$
▽	1·1	7·3	10·3
✳	1·7	7·3	12·9
+	2·1	2·0	14·3
△	2·2	5·0	14·5
⊙	2·4	0·8	15·0
⊡	4·4	7·3	20·4

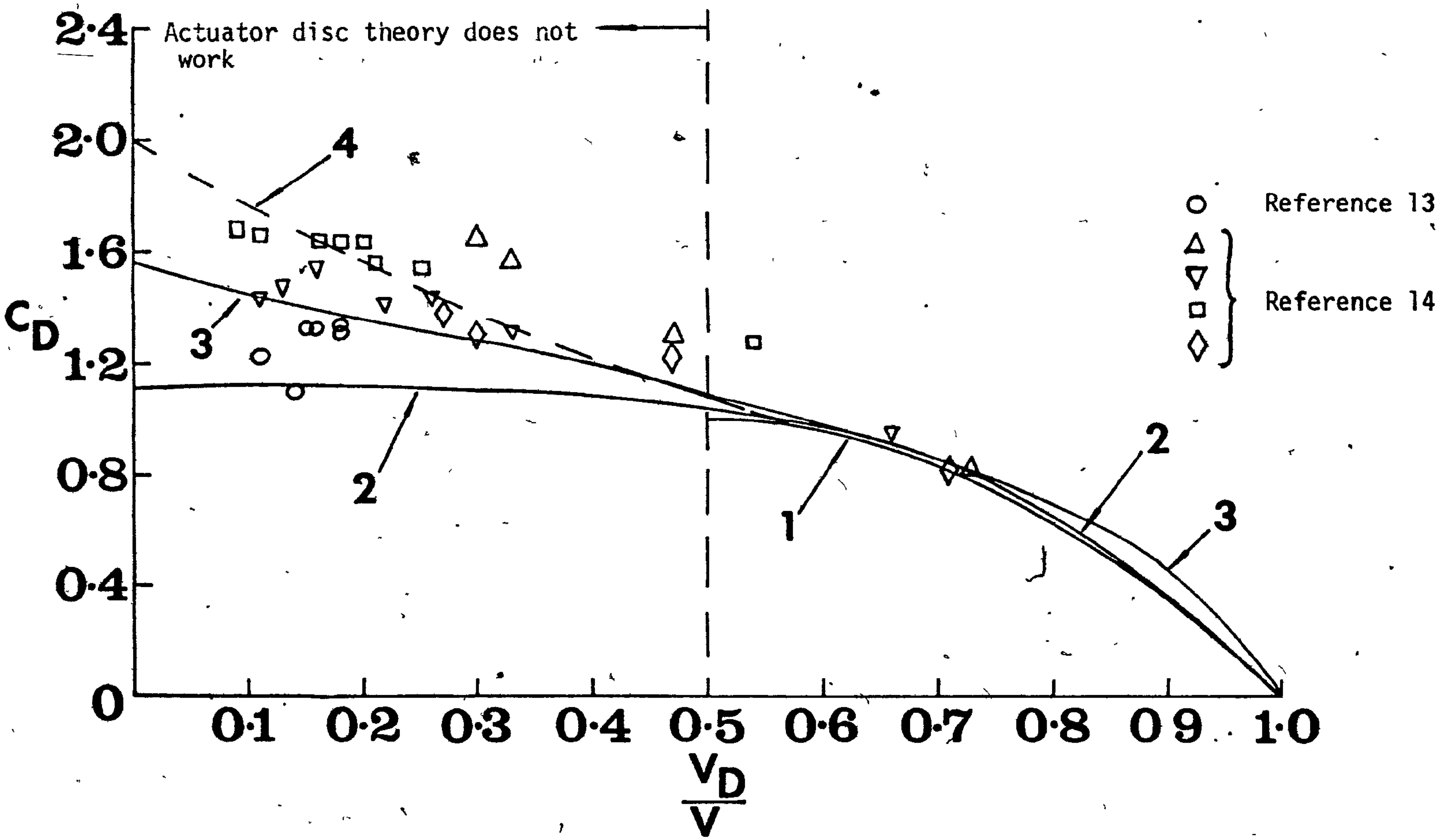

Figure ~~13~~ Drag coefficient plotted against disc velocity ratio according to the Actuator Disc theory and also three extensions to the theory

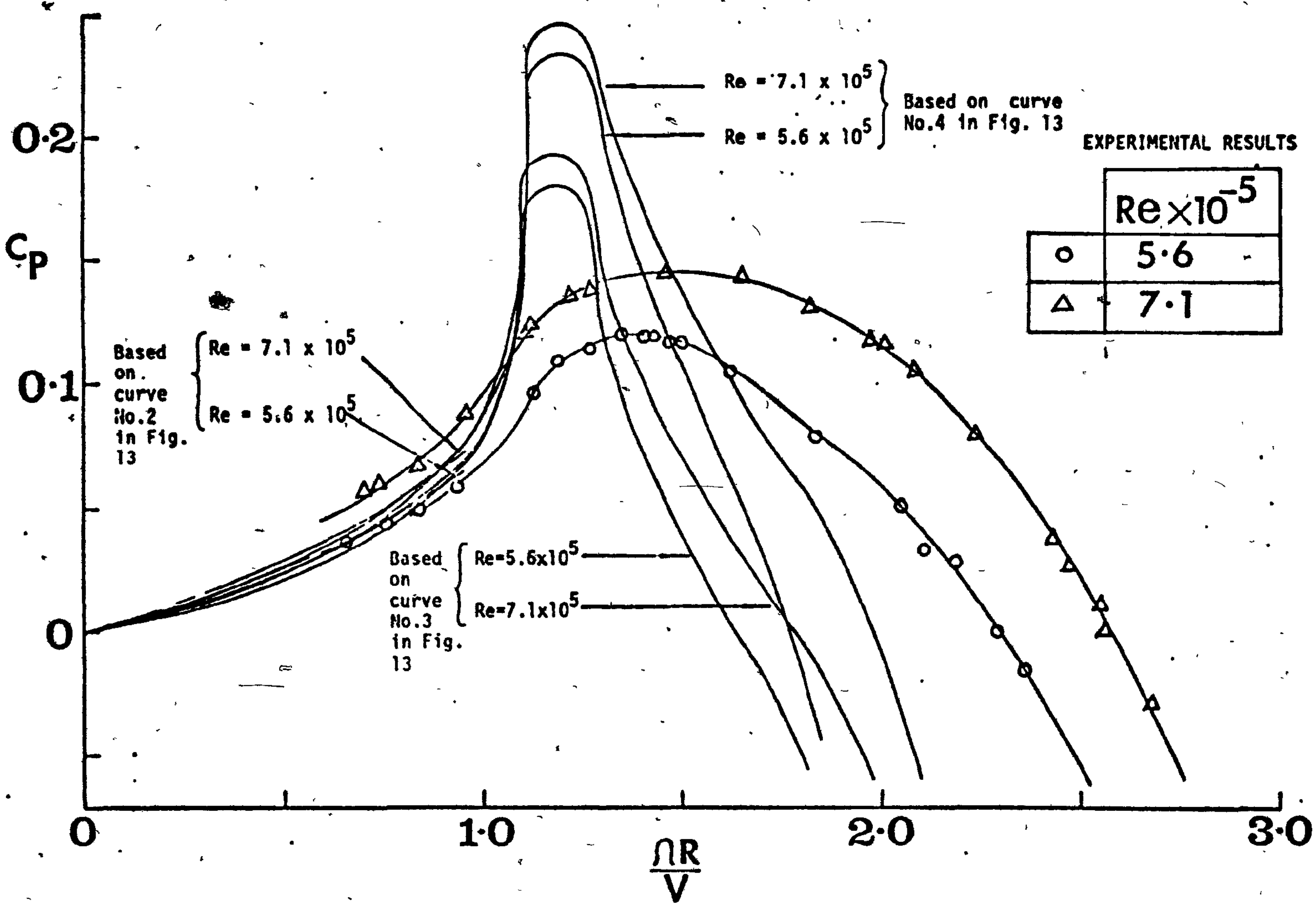

Figure 14 Power coefficient plotted against tip speed ratio for the double sail blades C_{TT}>14, compared with theoretical results based on extensions to the Actuator Disc theory at two Reynolds numbers

APPENDICES

APPENDIX A

Analysis for Sail Distortion

A sail of rectangular shape with uniform chord c, length b and a trailing edge hollow x is considered for simplicity: it is shown below in Fig. A-1:

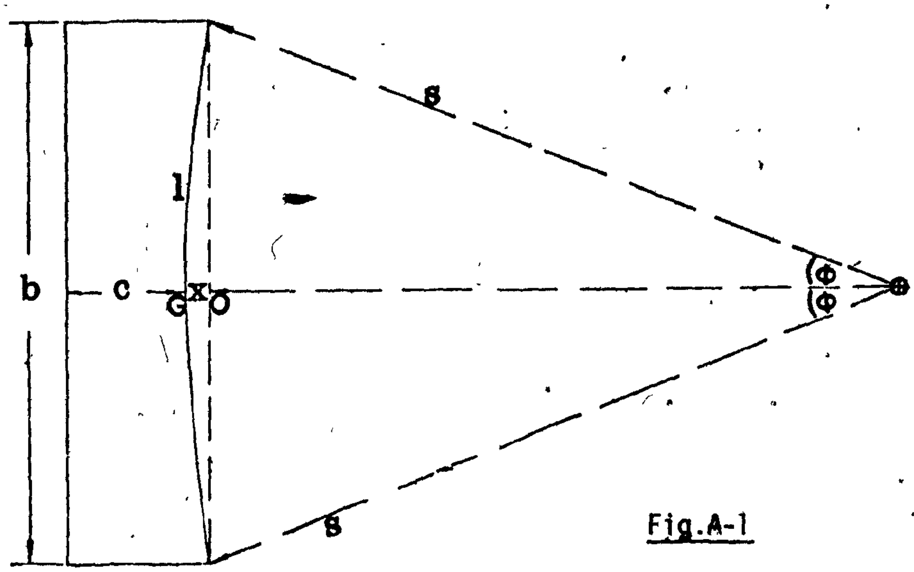

Fig.A-1

Taking the trailing edge as a circular arc of length ℓ and radius of curvature s.

From geometry:

$$s^2 = \left(\frac{b}{2}\right)^2 + (s-x)^2$$

$$s^2 = \frac{b^2}{4} + s^2 - 2sx + x^2$$

$$\therefore \frac{2s}{b}\,\frac{x}{b} = \frac{1}{4} + \left(\frac{x}{b}\right)^2$$

for small $\frac{x}{b}$, $x \doteq \frac{b^2}{8s}$ (A.1)

From geometry, $\sin\phi = \frac{b}{2s}$ (A.2)

Also $\ell = 2\phi s$

$$\therefore \phi = \frac{\ell}{2s} \qquad \text{(A.3)}$$

Substituting (A.3) into (A.2) gives

$$\frac{b}{2s} = \sin(\frac{\ell}{2s}) \tag{A.4}$$

Applying a sine expansion to equation (A.4) and approximating to 2 terms,

$$\frac{b}{2s} = \frac{\ell}{2s} - \frac{1}{3!}\left(\frac{\ell}{2s}\right)^3 + \ldots$$

$$b = \ell - \frac{\ell^3}{24s^2}$$

$$\frac{\ell}{b} = 1 + \frac{\ell}{24b}\left(\frac{\ell}{s}\right)^2 \tag{A.5}$$

Substituting for s from (A.1) into (A.5) and noting $(\frac{\ell}{b})^3 \doteqdot 1$,

$$\frac{\ell}{b} = 1 + \frac{8}{3}\left(\frac{x}{b}\right)^2 \tag{A.6}$$

If T is the tension in the leech, the chordwise force acting in the direction GO is T/s per unit length of sail.

The sail distortion under wind load in plan view is as shown in Fig. A-2:

Fig. A-2

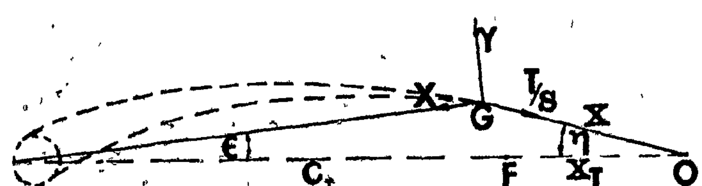

F is the original position of the trailing edge after pre-tension and x_T the original value of the leech hollow. X and Y are chordwise and normal components of the force on the trailing edge per unit length of sail. The angles ε and η are small.

Resolving forces along the chord gives

$$X = \frac{T}{s}\cos(\varepsilon+\eta) \tag{A.7}$$

For small ε and η equation (A.7) reduces to

$$X = \frac{T}{s} \tag{A.8}$$

Resolving forces perpendicular to the chord gives

$$Y = \frac{T}{s}\sin(\varepsilon+\eta) \tag{A.9}$$

For small ε and η, equation (A.9) reduces to

$$Y = \frac{T}{s}(\varepsilon+\eta) \tag{A.10}$$

Combining (A.8) and (A.10)

$$\varepsilon+\eta = \frac{Y}{X} \tag{A.11}$$

Putting $X = \frac{1}{2}\rho U^2 c C_X$ and $Y = \frac{1}{2}\rho U^2 c C_Y$ where C_X and C_Y are force coefficients and U is the net air velocity relative to blade section.

$$\eta+\varepsilon = \frac{C_Y}{C_X} \tag{A.12}$$

From Fig. A-2

$$x\sin(\eta+\varepsilon) = (c+x_T)\sin\varepsilon$$

$$(\eta+\varepsilon) = \left(\frac{c+x_T}{x}\right)\varepsilon \tag{A.13}$$

Substituting for $\eta+\varepsilon$ in (A.12)

$$\varepsilon = \left(\frac{x}{c+x_T}\right)\frac{C_Y}{C_X} \tag{A.14}$$

Equation (A.14) gives the change in incidence due to distortion.

If T_T is the pre-tension force in the leech and E_T is the force in the leech required to produce unit strain in it, then

$$T_T = E_T\left(\frac{\ell_T-\ell_0}{\ell_0}\right) \tag{A.15}$$

where

ℓ_0 is the unstretched length of the leech

ℓ_T is the length of the leech after pre-tension

T is the tension in the leech with wind load.

Then,
$$T = E_T\left(\frac{\ell-\ell_0}{\ell_0}\right) \tag{A.16}$$

Combining (A.15) and (A.16) to eliminate ℓ_0 and re-arranging we get

$$T = T_T + (T_T+E_T)\left(\frac{\ell}{\ell_T} - 1\right) \tag{A.17}$$

Combining (A.8) and (A.17) gives

$$X = \frac{1}{s}\left[T_T + (T_T+E_T)\left(\frac{\ell}{\ell_T} - 1\right)\right] \tag{A.18}$$

Substituting for s from (A.1) into (A.18)

$$X = \frac{8x}{b^2} T_T \left[1 + \left(1 + \frac{E_T}{T_T}\right)\left(\frac{\ell}{\ell_T} - 1\right)\right] \tag{A.19}$$

From (A.6) we can write

$$\frac{\ell}{b} = 1 + \frac{8}{3}\left(\frac{x}{b}\right)^2 \quad \text{and} \quad \frac{\ell_T}{b} = 1 + \frac{8}{3}\left(\frac{x_T}{b}\right)^2$$

Hence substituting for ℓ and ℓ_T into (A.19), we get

$$X = \frac{8x}{b^2} T_T \left[1 + \left\{1 + \frac{E_T}{T_T}\right\}\left\{\frac{1+\frac{8}{3}\left(\frac{x}{b}\right)^2}{1+\frac{8}{3}\left(\frac{x_T}{b}\right)^2} - 1\right\}\right] \tag{A.20}$$

By definition,

$$T_T = \frac{1}{2}\rho 2bcV^2C_{TT}$$

and

$$X = \frac{1}{2}\rho cU^2C_X$$

U^2, obtained from a vectorial addition of the velocity vectors on the wind turbine blade section, is averaged over one complete revolution of the turbine and the mean of the squares of the turbine radii. Therefore,

$$U^2 = V^2 + (\Omega r_m)^2 \tag{A.21}$$

where $r_m^{\ 2}$ is the mean of the squares of the wind turbine radii. Re-arranging equation (A.21) gives,

$$U^2 = V^2 + (\Omega R)^2\left(\frac{r_m}{R}\right)^2 \tag{A.22}$$

From the turbine geometry, (Fig. 1),

$$\frac{r_m^{\ 2}}{R^2} = \frac{2}{5}$$

Substituting the ratio $\frac{r_m^{\ 2}}{R^2}$ in equation (A.22), we get,

$$U^2 = V^2\left[1 + \frac{2}{5}\lambda^2\right] \quad \text{since } \frac{\Omega R}{V} = \lambda \tag{A.23}$$

Substituting for X and T_T in (A.20) we now get

$$\left[1 + \frac{2}{5}\lambda^2\right] C_X = \frac{8x}{b^2}\cdot 2bC_{TT}\left[1 + \left\{1 + \frac{E_T}{T_T}\right\}\left\{\frac{1+\frac{8}{3}(\frac{x}{b})^2}{1+\frac{8}{3}\left(\frac{x_T}{b}\right)^2} - 1\right\}\right] \quad \ldots \text{(A.24)}$$

Expanding (A.24) gives

$$\left(1 + \frac{2}{5}\lambda^2\right) C_X = C_{TT}\ 16\left(\frac{x}{b}\right)\left[1 + \left\{1 + \frac{E_T}{T_T}\right\}\left\{\frac{\frac{8}{3b^2}(x+x_T)(x-x_T)}{1 + \frac{8}{3}\left(\frac{x_T}{b}\right)^2}\right\}\right] \tag{A.25}$$

For small $\frac{x_T}{b}$ and $\frac{x-x_T}{b}$ equation (A.25) becomes

$$\left(1 + \frac{2}{5}\lambda^2\right) C_X = C_{TT}\ 16\ \frac{x_T}{b}\left[1 + \left\{1 + \frac{E_T}{T_T}\right\}\left\{\frac{16x_T}{3b^2}(x-x_T)\right\}\right] \tag{A.26}$$

The approximate change in chord of the sail becomes

$$\frac{x-x_T}{b} = \frac{\frac{b}{16x_T}\left(1 + \frac{2}{5}\lambda^2\right)\frac{C_X}{C_{TT}} - 1}{\left(1 + \frac{E_T}{T_T}\right)\frac{16x_T}{3b}} \tag{A.27}$$

APPENDIX B

Power Absorbed by Central Supporting Struts

Consider one strut of constant chord c and length R as shown in Fig. B-1. Ignore any aerodynamic interference between the struts.

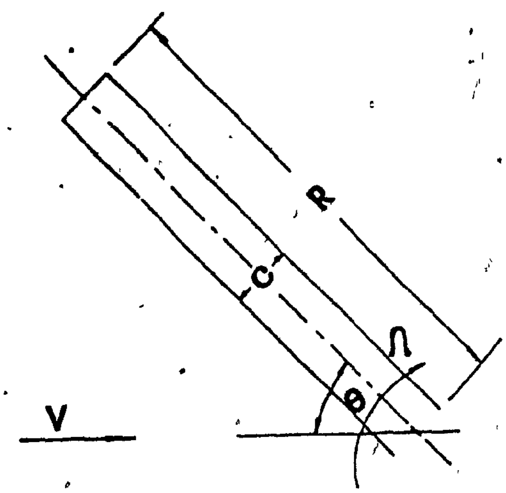

Fig. B-1

Assume c << R. The drag coefficient C_D of the strut section is taken to be constant and the drag dependent only on the velocity normal to the leading edge.

At radius r, the drag per unit span on one strut in the direction of the normal velocity component

$$D = \frac{1}{2} \rho c C_D [V\sin\theta - \Omega r]^2 \tag{B.1}$$

Hence work done against drag through a small angle dθ, for a strip dr of the strut is

$$dW = - \frac{1}{2} \rho c C_D [V\sin\theta - \Omega r]^2 \, r d\theta \cdot dr \tag{B.2}$$

Therefore work done through one revolution opposing rotation

$$W = -\frac{1}{2}\rho c C_D \int_0^R \int_0^{2\pi} (V\sin\theta - \Omega r)\,|V\sin\theta - \Omega r|\; r d\theta \cdot dr$$

$$= \frac{1}{2}\rho c C_D \int_0^R \int_0^{2\pi} \pm\left[V^2\sin^2\theta - 2V\sin\theta\Omega r + \Omega^2 r^2\right] r d\theta \cdot dr \qquad \text{(B.3)}$$

when $\Omega r > V\sin\theta$, W is positive.

Rearranging (B.3) gives

$$W = \frac{1}{2}\rho c C_D \int_0^R \int_0^{2\pi} \pm\left[V^2\left(\frac{1}{2} - \frac{1}{2}\cos 2\theta\right) - 2V\sin\theta\Omega r + \Omega^2 r^2\right] r d\theta \cdot dr \qquad \text{...(B.4)}$$

Because of the change of sign of the integrand, the integration with respect to θ is done first and in two parts:

$$W = \frac{1}{2}\rho c C_D \int_0^R \left[\left\{V^2\left(\frac{\theta}{2} - \frac{1}{4}\sin 2\theta\right) + 2V\cos\theta\Omega r + \Omega^2 r^2 \theta\right\}_0^{2\pi} - 2\left\{V^2\left(\frac{\theta}{2} - \frac{1}{4}\sin 2\theta\right) + 2V\cos\theta\Omega r + \Omega^2 r^2\theta\right\}_{\theta_1}^{\pi-\theta_1}\right] rdr$$

where

$$\sin\theta_1 = \frac{\Omega r}{V} \quad \text{when } \Omega r < V$$

$$= 1 \quad \text{when } \Omega r > V$$

After re-arranging

$$W = \frac{1}{2}\rho c C_D \int_0^R \left[\left(\frac{V^2}{2} + \Omega^2 r^2\right) 4\theta_1 - V^2\sin 2\theta_1 + 8V\Omega r\cos\theta_1\right] rdr \qquad \text{...(B.5)}$$

Putting $\frac{\Omega R}{V} = \lambda$, gives

$$W = \frac{1}{2}\rho c C_D \int_0^R V^2 \left[\left\{\frac{1}{2} + \lambda^2 \left(\frac{r}{R}\right)^2\right\} 4\theta_1 - \sin 2\theta_1 + 8\lambda\left(\frac{r}{R}\right)\cos\theta_1\right] r\,dr \quad \ldots(B.6)$$

Putting $z = \frac{r}{R}$, $\therefore dr = R dz$

$$\therefore W = \frac{1}{2}\rho c C_D V^2 \int_0^1 \left[\left\{\frac{1}{2} + \lambda^2 z^2\right\} 4\theta_1 - \sin 2\theta_1 + 8\lambda z \cos\theta_1\right] Rz\, Rdz$$

$$W = \frac{1}{2}\rho c C_D R^2 V^2 \int_0^1 \left[\left(\frac{1}{2} + \lambda^2 z^2\right) 4\theta_1 - \sin 2\theta_1 + 8\lambda z \cos\theta_1\right] z dz \quad \ldots(B.7)$$

where

$$\theta_1 = \sin^{-1} \lambda z \quad \text{when } \lambda z < 1$$
$$= \frac{\pi}{2} \quad \text{when } \lambda z > 1$$

Equation (B.7) is integrated in parts.

First Integral:

$$\int_0^1 2\theta_1 z\, dz = \int_0^{\pi/2} \frac{2\theta_1}{\lambda} \sin\theta_1 \frac{1}{\lambda} \cos\theta_1 d\theta_1 \quad \text{for } \lambda z < 1$$
$$+ \int_{1/\lambda}^1 \pi z\, dz \quad \text{for } \lambda z > 1$$
$$= \frac{1}{\lambda^2} \int_0^{\pi/2} \theta_1 \sin 2\theta_1 d\theta_1 + \underbrace{\left[\pi \frac{z^2}{2}\right]_{1/\lambda}^1}_{\lambda > 1}$$

After re-arranging

$$\int_0^1 2\theta_1 z\, dz = \frac{\pi}{4\lambda^2} + \frac{\pi}{2}\left\{1 - \frac{1}{\lambda^2}\right\} \quad (B.8)$$

the term in the parenthesis being applicable when $\lambda > 1$.

Second Integral:

$$\int_0^1 4\lambda^2\theta_1 z^3 dz = \int_0^{\pi/2} 4\theta_1\lambda^2 \frac{1}{\lambda^3}\sin^3\theta_1 \frac{1}{\lambda}\cos\theta_1 d\theta_1 + \int_{1/\lambda}^1 4\lambda^2 \frac{\pi}{2} z^3 dz$$

for $\lambda>1$

$$= \frac{1}{\lambda^2}\int_0^{\pi/2}\left[\theta_1 \sin 2\theta_1 - \frac{\theta_1}{2}\sin 4\theta_1\right] d\theta_1 + \underbrace{\frac{\pi\lambda^2}{2}\left\{1 - \frac{1}{\lambda^4}\right\}}_{\lambda>1}.$$

After rearranging and integrating we get

$$\int_0^1 4\lambda^2\theta_1 z^3 dz = \frac{5\pi}{16\lambda^2} + \frac{\pi\lambda^2}{2}\left\{1 - \frac{1}{\lambda^4}\right\} \tag{B.9}$$

the last term in the parenthesis being applicable when $\lambda>1$

Third Integral:

$$\int_0^1 z \sin 2\theta_1 dz = \int_0^{\pi/2} \frac{1}{\lambda}\sin\theta_1 \sin 2\theta_1 \frac{1}{\lambda}\cos\theta_1 d\theta_1 + \underbrace{\int_{1/\lambda}^1 z \sin\pi dz}_{\lambda>1}$$

$$= \frac{1}{2\lambda^2}\int_0^1 \left(\frac{1}{2} - \frac{1}{2}\cos 4\theta_1\right) d\theta_1.$$

$$= \frac{\pi}{8\lambda^2} \tag{B.10}$$

Fourth Integral:

$$\int_0^1 8\lambda z^2 \cos\theta_1 dz = \int_0^{\pi/2} 8\lambda \frac{1}{\lambda^2}\sin^2\theta_1 \cos\theta_1 \frac{1}{\lambda}\cos\theta_1 d\theta_1$$

$$+ \underbrace{\int_{1/\lambda}^1 8\lambda z^2 \cos\frac{\pi}{2} dz}_{\lambda>1}$$

$$= \frac{2}{\lambda^2}\int_0^{\pi/2}\left(\frac{1}{2} - \frac{1}{2}\cos 4\theta_1\right) d\theta_1$$

$$= \frac{\pi}{2\lambda^2} \tag{B.11}$$

Summing up the results from equations (B.8), (B.9), (B.10), and (B.11):

$$W = \frac{1}{2}\rho c C_D R^2 V^2 \left[\left(\frac{\pi}{4\lambda^2} + \frac{5\pi}{16\lambda^2} - \frac{\pi}{8\lambda^2} + \frac{\pi}{2\lambda^2}\right) + \left\{\frac{\pi}{2}\left(1 - \frac{1}{\lambda^2}\right) + \frac{\pi\lambda^2}{2}\left(1 - \frac{1}{\lambda^4}\right)\right\}\right]$$

where the term in parenthesis is applicable only when $\lambda > 1$.

Finally rearranging

$$W = \frac{1}{2}\rho c C_D R^2 V^2 \left[\frac{15\pi}{16\lambda^2} + \left\{\pi\left(1 - \frac{1}{\lambda^2}\right)\left(1 + \frac{\lambda^2}{2}\right)\right\}\right] \tag{B.12}$$

the last term in parenthesis being applicable when $\lambda > 1$.

Power, $P = \frac{NW\Omega}{2\pi}$ for N struts.

Hence, $\Delta Cp = \dfrac{P}{\frac{1}{2}\rho V^3 A} = \dfrac{NW\Omega}{\frac{1}{2}\rho V^3 A 2\pi}$

$$\Delta Cp = \lambda C_D\left(\frac{Nc}{R}\right)\frac{R^2}{A}\left[\frac{15\pi}{16\lambda^2} + \left\{\left(1 - \frac{1}{\lambda^2}\right)\left(1 + \frac{\lambda^2}{2}\right)\right\}\right] \tag{B.13}$$

the last term in parenthesis being applicable when $\lambda > 1$.